Mechanics of Electrified Interfaces in Diluted Electrolytes

Dissertation
zur Erlangung des Grades
des Doktors der Naturwissenschaften
der Naturwissenschaftlich-Technischen Fakultät II
- Physik und Mechatronik -
der Universität des Saarlandes

von

Maxim Smetanin

Saarbrücken

2010

Tag des Kolloquiums:	03.09.2010
Dekan:	Univ.-Prof. Dr. Christoph Becher
Vorsitzender:	Univ.-Prof. Dr. Ludger Santen
Mitglieder des Prüfungsausschusses:	Univ.-Prof. Dr. Jörg Weissmüller Univ.-Prof. Dr. Ralf Seemann
Akad. Mitarbeiter:	Dr. Michael Koblischka

Abstract

This work describes an experimental investigation of the interface between a solid metal and a fluid electrolyte. The question to be answered was: How does the surface stress vary with the surface charge density and how does the electrode potential vary with the elastic strain of the metal? The two variations are linked by the thermodynamic Maxwell relation that is well known but has not been tested in experiment. The aims of the thesis were twofold: First, to conduct careful experimental determination of the surface stress at electrode surfaces in aqueous electrolytes chosen to minimize the specific adsorption and thus to highlight selectively the role of capacitive processes. Second, to design and execute an experiment that allows for the first time to measure the variation of the electrode potential with the elastic strain. In the first approach, an *in situ* cantilever bending experiment was set up. The experiment shows that surface stress, f, varies linearly with the surface charge, q, with a response parameter $\varsigma = \mathrm{d}f/\mathrm{d}q = -2.0$ V. This value is larger, by the factor of two, than some previously reported experimental results. In the second approach, a new experimental approach was implemented, where the electrode is a metal film deposited on a polymer substrate and cyclic elastic strain of the electrode is imposed by straining the substrate via a piezoelectric actuator. This experiment supplies quantitative results for the potential – strain coupling. The value, $\varsigma = -1.83$ V, is in good agreement with the cantilever bending experiment and the *ab initio* work. Therefore, for the first time, the important thermodynamic Maxwell relation was experimentally verified.

Zusammenfassung

In dieser Arbeit wird die experimentelle Untersuchung der Grenzflächen zwischen einem festen Metall und einem flüssigen Elektrolyt beschrieben. Die zu beantwortende Frage war inwiefern sich die elastische Flächenspannung mit der Oberflächenladungsdichte verändert und wie das Elektrodenpotential mit der elastischen Dehnung des Elektrodenmetalls zusammenhängt. Diese beiden Beziehungen hängen über die thermodynamische Maxwell-Relation, die zwar in der Literatur wohlbekannt aber noch nie experimentell nachgewiesen wurde, zusammen. Demzufolge ergaben sich zwei Ziele dieser Arbeit: Erstens die sorgfältige Ausführung einer experimentellen Bestimmung der elastischen Flächenspannung an Elektrodenoberflächen in wäßrigen Elektrolyten, welche so ausgesucht sind, daß sie die spezifische Adsorption minimieren und somit die Rolle der kapazitiven Prozesse isolieren. Zweitens ein Experiment aufzubauen und durchzuführen, welches erstmalig die Messung der Veränderung des Elektrodenpotentials als Funktion der elastischen Dehnung ermöglicht. In einem ersten Ansatz wurde ein *in-situ* Balkenbiegeexperiment aufgebaut. Dieses Experiment hatte zum Ergebnis, daß die elastische Flächenspannung f linear von der Oberflächenladung q abhängt; die Steigung, hier auch „Response-Parameter“ genannt, betrug $\zeta = \mathrm{d}f/\mathrm{d}q = -2.0$ V. Dieser Wert ist um einen Faktor 2 höher als Werte, die in früheren Experimenten ermittelt wurden. In einem zweiten Ansatz wurde ein neuer experimenteller Zugang implementiert, in welchem die Elektrode ein Metallfilm ist, der auf einem Polymersubstrat deponiert wurde, und anschließend zyklischen elastischen Dehnungen ausgesetzt wurde, indem das Polymersubstrat mittels eines piezoelektrischen Stellantriebs verformt wurde. Der ermittelt Wert $\zeta = -1.83$ V ist in guter Übereinstimmung mit dem Balkenbiegeexperiment und den *ab-initio* Rechnungen. Dieses Experiment liefert quantitative Ergebnisse für die Kopplung zwischen Potential und Dehnung. Demzufolge wurde hier die wichtige thermodynamische Maxwell-Relation erstmalig experimentell verifiziert.

Acknowledgements

Here, I would like to thank all people who have helped me during the study and made my experience in the lab both educational and pleasurable.

It is difficult to overstate my gratitude to my supervisor PD Dr. Jörg Weissmüller. He, with his enthusiasm, inspiration, and ability to explain things clearly and simply, helped to make the work interesting and fruitful for me. Throughout my research, he provided encouragement, good teaching, sound advices, good company, and many interesting ideas. I heartily thank to him for keeping his door open every time I come to him for help and suggestions.

I wish to thank my group colleagues Dr. Dominik Kramer and Dr. Raghavan N. Viswanath for their scientific suggestions and encouragements during my research at Institute of Nanotechnology.

I gratefully acknowledge Prof. Dieter Kolb, Dr. Ludwig Kibler and Dr. Khaled Soliman who introducing me into the many aspects of experimental and theoretical electrochemistry.

I would like to express my large gratitude to Prof. Ulrich Herr and Dr. Senthilnathan Mohanan from the University of Ulm, Dr. Detlef Beckmann and Sheng Zhong from the Institute of Nanotechnology for the help in the samples preparation.

My appreciation also goes to Dr. Thomas Koch and Dr. Stefan Walheim who halped me to obtained professional AFM micrographs of my samples.

I sincerely appreciated Dr. Jürgen Markmann and Dr. Christian Lemier for fruitful discussions during my Ph.D. thesis writing.

Special thanks to Christine Batch, Erika Schütze and Dr. Olaf Wollersheim for taking care of official matters during my stay at Institute of Nanotechnology.

And many thanks to everyone who helped in any way contributing to this Ph.D. thesis.

Financial support from the Landesstiftung Baden-Württemberg and the Deutsche Forshungsgemeinschaft are gratefully acknowledged.

Finally, I want to thank my family for the patience, support and understanding.

Contents

1 Introduction 1

1.1 Thermodynamic Maxwell relation 2

1.2 Surface stress-charge response 3
1.2.1 Surface stress-charge coefficient 3

1.3 Electrode potential-strain response 5
1.3.1 Relevance for corrosion 5

1.4 Outline 6

2 Theoretical description of the solid-electrolyte interface 9

2.1 Definition of a Surface stress 9

2.2 Wafer bending technique for the measurements of the surface stress variation 10

2.3 Double layer, electrified interface 10
2.3.1 Faradaic processes 11
2.3.2 The ideal polarized electrode 12
2.3.3 Electrical double layer 12
2.3.4 Potential of zero charge 13

2.4 Relation of the electrode potential to the work function 14

3 Experimental procedure 15

3.1 Sample preparation 15
3.1.1 Au on (100) silicon wafers 15
3.1.2 Au thin films on Kapton foil 15

3.2 Sample Characterization: X-ray, AFM 15

3.3 Experimental setup of the surface stress measurement combined with electrochemical setup 16
3.3.1 Surface stress measurements at the metal-electrolyte interface 17
3.3.2 The electrochemical cell 19
3.3.3 Experimental measurement potential of zero charge at metal-electrolyte interface 20

3.4 Experimental methods of the electrode potential response to an elastic strain measurement 21
3.4.1 Experimental setup for measurements of potential-elastic strain response of a metal wire: Balance method 22
3.4.2 Experimantal concept for the measurements of the potential-elastic strain response of a metal film 22
3.4.3 Mechanical arrangements of the cyclic elastic strain 23
3.4.4 Sample mounting into the tension apparatus 24
3.4.5 The inert gas chamber 26
3.4.6 Installation the sample into the tension apparatus 26
3.4.7 Measurement of electrode potential-elastic strain response 27

4 Results 29

4.1 Microstructure of the gold electrodes 29

4.2 Potential of zero charge of the (111)-textured gold electrode in aqueous solutions of NaF and $HClO_4$ 30

4.3 Surface stress of (111) textured Au film in diluted aqueous electrolytes 31
4.3.1 Anisotropic aspects in the detection of the wafer bending 31
4.3.2 Experimental measurements of the surface stress of (111)-textured gold electrode in aqueous solution of NaF 32

4.3.3 Measurement of the surface stress of (111)-textured gold electrode in aqueous solution of $HClO_4$ 33
4.3.4 Reproducibility in wafer bending experiment 35
4.4 Open circuit potential-strain response of Pt wire in aqueous solution of H_2SO_4 36
4.5 Open circuit potential-strain response of the Au film in aqueous solution of $HClO_4$ 37
4.5.1 Cyclic voltammogram of the Au electrode 37
4.5.2 The electrode potential of a (111)-textured Au film as the function of the cyclic elastic strain 37
4.5.3 Open circuit potential response at different frequencies of elastic strain of a (111)-textured Au film measured in aqueous solution of $HClO_4$ 38
4.5.4 Open circuit potential-strain coefficient as a function of strain frequency of a (111)-textured Au electrode in aqueous solution of $HClO_4$ 39
4.5.5 Interpretation of the results for the $\delta E_{oc}/\delta e$ coefficient using an equivalent electrical circuit 40

5 Discussion 43

5.1 The surface stress-charge coefficient of (111)-textured Au electrode in specifically nonadsorbing diluted aqueous electrolytes 43
5.1.1 Magnitude of surface stress-charge coefficient 43
5.1.2 Presence of specific anion adsorption at the electrode 43
5.1.3 Intrinsic surface stress-charge coefficient; role of charge transfer at metal-electrolyte interface 44
5.1.4 Surface stress-potential response 46
5.1.5 Roughness contribution to the measured surface stress 46
5.1.6 Summary of the charge effect on the surface stress 47
5.2 Electrode potential-strain response 48
5.2.1 Electrode potential-strain response in an aqueous electrolyte contained metal ions 48
5.2.2 Electrode potential-strain response in a blank electrolyte 50
5.2.3 Summary of potential-strain response results 50

6 Summary 51

7 Outlook: Potentiostatic measurement of the potential-strain response 53

Symbols 55

References 57

1 Introduction

A central issue in the electrochemistry is an electric double layer at a metal-electrolyte interface. Helmholtz [1] described this double layer as plate capacitor of a molecular dimension. The one plate is the metal surface and the other plate is formed by solvated ions at closest approach to the metal surface. A main part of the existing knowledge about the properties of the metal-electrolyte interface is based on the measurements of the surface tension, γ. The surface tension is the *work required to increase* the surface area of a fluid. Gibbs [2] established the thermodynamic description of the metal-electrolyte interface, relating the surface tension, the adsorption and the electrochemical potential. From the electrochemical experiments with a mercury droplet in the contact with an electrolyte Lipmann [3] showed that the surface tension of mercury is a quadratic function of the electrode potential. Gouy [4] and Chapman [5] significantly deepened the Helmholtz theory of the electric double layer. They proposed that the ionic charge of the double layer forms a diffuse layer near the metal surface.

Later, representations of the metal-electrolyte interface by Gibbs, Lipmann, Gouy and Chapman were applied to solid electrodes. In the case of solids, it is important to make distinction between the surface tension and the surface stress, *f*. The surface stress of a solid surface measures *the work required for an elastic deformation of the surface in its tangential plane*. Although, the surface stress and the surface tension are similar in liquid-gas or liquid-liquid interfaces but they are very different in solid-gas or solid-liquid interfaces. Studying and understanding the causes of surface stress changes in electrochemical systems presents a significant challenge, because there are always a variety of processes occurring at a solid-liquid interface. The chemical interaction of ions with the metal surface, the charge transfer processes and the effect of a space charge within the double layer can not be easily differentiated. These processes largely determine the electrode behaviour and could be equally attributed as the main factors which affecting the state of the surface and particularly the surface stress [6]. Therefore, it is necessary to understand how the different electrode processes – e.g. charging the electrode surface through the double layer or adsorption of ions – influence the surface stress response of the metal.

The surface energy-conjugated variable to the surface stress is the elastic strain of solids. Such strain has been shown to modify the chemisorption properties of the metal considerably [7,8]. If strain generally induces changes in the ability of a surface to form bonds to adsorbed atoms or molecules, the possibility arises of using strain to manipulate the reactivity of a metal [9]. However, there is no experimental data with quantitative information on the dependency of the electrode potential from the elastic strain of the surface.

Therefore, the aims of the thesis were twofold. First, conduct careful experimental determination of the surface stress at electrode surfaces in aqueous electrolytes. Second, to design and execute an experiment that allows for the first time to measure the effect of the elastic strain on the electrode potential. In the first approach, by means of the cantilever-bending technique the surface stress changes were examined as a function of the electrode potential and surface charge. In order to highlight the role of capacitive processes in the surface stress specifically non-adsorbing aqueous

electrolytes were chosen. Therefore, the results clearly represent the surface stress dependency from the intrinsic charge accumulated at the metal surface. This provides the quantitative estimation of the surface stress-charge coefficient, an important thermodynamic parameter. The newly obtained values for the surface stress-charge coefficient by a factor of two larger than previously published experimental results [10]. Agrees with theoretical *ab-initio* calculation [11,12]. This is suggesting a dominant role of the intrinsic charge over the change in the surface stress.

Furthermore, thermodynamics suggest an independent approach for verifying the results of cantilever-bending experiments. Thermodynamic Maxwell relation showed that the surface stress-charge coefficient is equal to the electrode potential changes occur during an elastic strain of the electrode. So far, no accepted measurement of the electrode potential-strain response has been reported. Therefore, in order to measure the electrode potential-elastic strain response a new experimental approach was developed. With the new experimental setup, the electrode potential-elastic strain response was quantitatively measured for the first time at the metal-electrolyte interface. The new results confirmed quantitatively the results of the cantilever bending experiments as well as *ab initio* computation [11,12]. Thus, for the first time a unified picture of the coupling between mechanics of electrodes and their electrical property evolves. What is more, the Maxwell relation as a fundamental thermodynamic relation for electrodes is for the first time confirmed by experiment.

The subsequent chapters display the state of the art in the relevant fields in more detail.

1.1 Thermodynamic Maxwell relation

Thermodynamic Maxwell relation proposes the symmetry between mechanical and electrical works. This statement formulated more then 40 years ago by Gokhshtein [13] was not yet proved experimentally. The energy-conjugate quantity to the surface stress, f, is the elastic strain, e. Considering a surface free energy density, $\psi(q,e)$, which is a state function, the corresponding state variables are the interfacial charge density, q, and the elastic strain. The conjugate variables to q is the electrode potential, E. The differential of the surface free energy:

$$\mathrm{d}\psi = E\mathrm{d}q + f\mathrm{d}e\,. \tag{1.1}$$

By using the well known relation between derivatives of a state function in respect to the state variables, namely

$$\frac{1}{\partial x_i}\left(\frac{\partial \psi}{\partial x_j}\right) = \frac{1}{\partial x_j}\left(\frac{\partial \psi}{\partial x_i}\right)$$

one obtain here:

$$\left.\frac{\partial f}{\partial q}\right|_e = \left.\frac{\partial E}{\partial e}\right|_q . \tag{1.2}$$

This relation equates responses of the surface stress-charge density, df/dq, with the electrode potential-elastic strain, dE/de. Different groups studied the derivation df/dq for various systems [10,17], but even the interpretation of a general behaviour is still diverse in the literature. Concerning the right part of Eq. 1.2, there is no clear and quantitative experimental data up to now. For better understanding of the

thermodynamics of a metal-electrolyte interface, rigorous studies the effects of an elastic strain on an electrode potential as well as a surface stress-charge dependency are required.

1.2 Surface stress-charge response

During the last decade, has been increased interest in the surface stress of metal electrodes. Possible sensor [14- 17] and actuator [18,19] applications of surface stress have been not only suggested and demonstrated but even commercialized in the case of sensors [20]. New experimental methods have been developed, which allow measurements of the surface stresses induced by sub-monolayer quantities of adsorbates on well defined metal [21] and semiconductor [22] surfaces in an ultrahigh vacuum and in a liquid electrolyte [23,24]. The understanding of the surface stress origin of the metal in electrolyte was advanced by recent publications on the thermodynamics [25] and on *ab initio* calculations of charged surfaces and strain [11,12]. The response of surface stress to changes in the excess charge density relates to fundamental issues in electrochemistry, such as electron transfer in surface-adsorbate bonds or microscopic processes in the electrochemical double layer [6,26]. It was shown previously that the surface stress response is stronger when there is less adsorption [10,27]. These results suggest that the surface excess charge, q, is a decisive factor for the changes of the surface stress [10,27]. Yet, the microscopic processes linking q to forces and relaxation at metal surfaces are poorly understood.

1.2.1 Surface stress-charge coefficient

Gokhshtein [13] and Beck [28] have conducted the first experimental measurements of surface stress of a solid at metal-electrolyte interface. Many publications, especially most of those published before 1998, describe the dependence of surface stress of solids as compatible to that of the surface tension, γ. Often, experimentally observed parabolas [28] of the surface stress were described as analogous to the surface tension[28]. If for the liquid metal it is true due to the absence of the shear stress, in the case of the solid metal the surface tension and the surface stress are two different parameters. The work of Haiss *et al*. [10] made important contribution by demonstrating a linear dependence of the surface stress from the charge, $f(q)$, whereas γ varies with the square of the charge density, according to the Lippmann equation:

$$\mathrm{d}\gamma/\mathrm{d}E = -q. \qquad 1.3$$

By integrating the surface tension one gets quadratic relation between γ and the charge, $\Delta\gamma \sim q^2$. In the following years, the linear $f(q)$ behaviour was experimentally confirmed by different groups [10,21,6,29]. However, no agreement was reached on the values of the surface stress-charge coefficient, $\mathrm{d}f/\mathrm{d}q$. Experimentally, for planar electrodes, $\mathrm{d}f/\mathrm{d}q$ values [10] for the metal-electrolyte interface were measured in the order of –1 V while theoretically for the case of the charged surface in a vacuum a value of –1.89 V was predicted [11]. In the case of a nanoporous metal immersed into an aqueous electrolyte, the surface stress-charge coefficient was obtained in the order of –2 V [27].

The noticeable disagreement in the values of the coefficient obtained by the different methods [10,11,17,27] is possible to attribute to the nature of electrolytes, metals and electrode topologies. However, in the DFT calculations [11] the influence

of a charge alone on the surface stress was considered. The difference between those experimental and the theoretical results might be due to the presence of charge transfer during specific anion adsorption. Ions become specifically adsorbed when short-range interactions between them and the metal surface become important. The charge transfer occurs during the specific adsorption decreasing the intrinsic charge in the metal. This is also supported by the fact that the value of df/dq is decreasing with increasing strength of the anion adsorption. The reported values of Haiss et al. [10] for df/dq of a (111) oriented gold surface measured for different anions ClO_4^-, SO_4^-, Cl^- and Br^- were –0.91 V, –0.85 V, –0.67 V, –0.45 V respectively. It was seen that the coefficient decreasing with increase of the anion affinity for the specific adsorption on the electrode surface. Recently, the influence of the concentration of the electrolyte on the surface stress was investigated by Viswanath et al [27]. They performed the experiment with dilution series of the aqueous electrolyte. It was found, that df/dq value of the platinum nanoporous electrode in aqueous NaF, was increasing with decrease of electrolyte concentration and approaches the value of –2 V[27]. Both experimental observations suggest the following conclusion: The higher the adsorption strength of an electrolyte the more charge is expected to transfer between ions and metal, and the less is the surface-stress-charge coefficient. A correlation of the surface stress-charge coefficient with charge transfer processes is possible. Consequently, the contribution of a capacitive charge at a metal-electrolyte interface to the surface stress is probably a decisive factor.

Therefore, a capacitive charge in the electric double layer is the main parameter which influence the surface stress. The statement that can be proved if the charge transfer processes are excluded. This can provide the better understanding of the microscopic origin of the surface stress-charge response. However, bonds with adsorbates [6,30] change the water dipole orientation [31] and the charge [11,12] has all been suggested to influence or even dominate the surface stress of a metal. The overall picture concerning surface stress is following: variations of f in an electrolyte that allows changing and controlling the surface charge directly are explained by ion adsorption. Variations of f in an electrode adjacent to a gas phase, where the charge within the metal can not be controlled or measured, are explained by surface charge effects [6]. More reliable experimental numbers might help in clarifying this issue.

It is important to have adequate numbers for the df/dq since it could give possibility to quantify an amount of the charge which leaks through the metal-electrolyte interface during the specific anion adsorption. In other words, it can give the opportunity to estimate an amount of specifically adsorbed ions and the electrosorption valency [32]. Until now, the quantitative estimation of these parameters was not accessible by experiments. However, these parameters are important for further understanding of fundamental properties of a metal-electrolyte interface.

Recently Weissmüller and Duan [33] calculated the effect of the surface topology on the measured surface stress value. Their theoretical work shows that the measured surface stresses, depending on the roughness of an electrode should differ from an intrinsic surface stress of the metal surface. The important parameter in this respect is the surface roughness. In some instances the measured surface stress value could be underestimated by 10 % if surface roughness is not taken into account. This point has to be taken into account while evaluating df/dq values obtained from the experiment. Obviously, a rigorous characterization of the surface topology is important for the correct evaluation of the surface stress coefficient.

1.3 Electrode potential-strain response

The fact that the elastic strain affecting the electric properties was known for a long time. The change of the electric resistance of metallic wires with elastic strain was first investigated by Lord Kelvin [34] in 1856. It was utilized later in the operation of electrical-resistance gauges [35].

The elastic strain couples to surface science in as much as its invention provide a better understanding of the properties of the metals surfaces. The elastic strain determines the catalytic reactivity [9,36-39 and corrosion behaviour [44,45,40,-42,] of the metals. The interplay of mechanical and electrochemical effects has been a field of detailed studies in recent years [6-11,15,43-45]. In the relevant experiments, as it was discussed in the previous paragraphs, the electrode potential is most often controlled and the mechanical strain of the surface is the observed quantity. At the solid-electrolyte interface, the electrode potential is closely related to the work function [46,47]. Little is known about the dependency of the electrode potential from the variation of the interatomic distances of surface atoms at the solid-electrolyte interface. Yet, while predictions from state of-the-art *ab initio* work are available [11,12] direct experimental studies of dE/de are scarce.

The recent suggestion that catalytic activity of a metal should couple significantly to the elastic strain via changes of the electronic density of states has prompted a renewed interest in the issue. Norskov *et al*. [9] proposed that elastic strain can change the reactivity of a metal by varying its work function. Kolb *et al.* [36] showed in an experimental work that the oxidation- reduction- potential of Pd monolayer is shifted due to a misfit strain. In this experiments, the elastic strain was achieved by the electrodeposition of one monolayer of Pd on top of the different single crystal metal surfaces. They found the shifts in potentials of hydrogen reduction and formic acid oxidation on the strained Pd adlayers. The values of the potential shifts were correlated with the values of the misfit strain of Pd adlayers. However, not only the mechanical strain but also the coupling between the electronic structure of the substrate bulk and the strained Pd adlayer could contribute to the measured potential shifts. Considering the difficulty of analysis of such an experiment it would be favourable to apply the elastic strain to the bulk metal itself and to measure correspondent shifts of the *pzc* or the oxidation-reduction potentials.

1.3.1 Relevance for corrosion

The relation of the elastic strain to the electrode potential has been topic of interest for a long time. The corrosion problem in structural materials under load [44,45], the stress corrosion cracking [48] are the most pressing problems nowadays. It is closely connected to the interrelation between mechanical and electrochemical processes. Fryxell and Nachtrieb [44] studied the effect of strain on the electrode potentials of silver and gold in contact with the electrolytes containing the corresponding metal ions. They demonstrated that tensile stress of a gold wire in 0.6 M $HAuCl_4$ shifts the electrode potential negatively, while compression of a gold cylinder shifts the electrode potential positively. For the silver in 0.1 M $AgNO_3$ they found the opposite dependency of the electrode potential from the elastic strain. Finally, they showed that two in principle similar metals, Au and Ag, electrochemically behaved differently. The potential-strain response, dE/de, was negative in the case of gold and positive in the case of silver. Later, Horvath and

Schiller [45] had confirmed the observation of Fryxell and Nachtrieb concerning the positive potential-stress response for the silver metal. They reported a value of the potential to strain coefficient, $\partial E/\partial e$, +1 V, for different Ag^+ ion concentrations in the electrolyte.

The presence of the metal ions in the solution provides a fast exchange current, i.e. the equilibrium is reached by means of constant electrochemical potential. The condition for equilibrium is different if a solvent contains no metal ions. In that case, the electrochemical potential is ill defined within the double layer. So far, no experimental observations of an open circuit potential response to an elastic strain for a system where the electrolyte does not contain metal ions were reported. Yet, the experimental situation stands in striking contradiction to the fundamental importance of this parameter.

1.4 Outline

The primary objectives of this work were to explore the metal-electrolyte interface: Namely, explore the physical origin of the surface stress variation, and the coupling between the electrode potential and the elastic strain. Two alternative experimental methods were used. The surface stress of a gold film is measured *in situ* as the function of the electrode potential and the charge density by means of a cantilever-bending method combined with the electrochemical cell. The relation between the electrode potential and the elastic strain was studied with the new experimental method. The metal electrode is subjected to the cyclic strain, and the potential measured using lock-in technique. This method allows the quantitative measurement of the electrode potential response to the elastic strain, for the first time. Data obtained from these two experimental methods proved the thermodynamic Maxwell relation for the first time.

In this work the surface stress-charge coefficient of (111) textured gold films is measured in dilute aqueous solutions of sodium fluoride and perchlorate. These electrolytes were chosen since they are considered as weakly adsorbing on gold surfaces and therefore specific adsorption is substantially minimized.

In order to carry out the measurement of the electrode potential-elastic strain response new experimental technique was developed, where the elastic strain was applied cyclically to the electrode. This allows to examinate the $dE/de|_q$ values at the different frequencies of the elastic strain. Thereby an estimation of the time-scale of faradaic and double layer processes at the metal-electrolyte interface was done.

The structure of this thesis is the following. The second chapter gives a detailed definition of the surface stress and background information regarding the electrochemical aspects of the metal-electrolyte interface. The third chapter describes the methods and the samples preparation. It also gives detailed information on the principles of the cantilever bending method, which allows in combination with the electrochemical method to determine the surface stress as a function of the charge density. This chapter also gives a detailed description of the potential-elastic-strain method. This approach which was developed by the author, provides clear information about the potential of zero charge dependency from the elastic strain. The main results of the work are presented in the forth chapter and discussed in the fifth. The sixth chapter summarized the achieved results. The seventh chapter gives an

outlook for the future implication of the developed method for the potential-elastic strain measurement during the cyclic voltammogram.

2 Theoretical description of the solid-electrolyte interface

2.1 Definition of a Surface stress

Changes of the superficial charge density or the density of adsorbed species at the solid-electrolyte interface give rise to forces at the surface which – at equilibrium– must be balanced by stresses in the underlying bulk. Three concepts are of importance for capillary phenomena [25]: *i*) the various specific surface excess free energies, representing the excess per area of the materials free energy over that of the matter in a suitable reference state, *ii*) the surface tension, *i.e.* the force per length of perimeter required for reversibly changing the surface area by adding matter to the constant structure, and, *iii*) the surface stress, which is a measure for the tendency of the surface to change its area by elastically deforming the underlying bulk phase. Gibbs [49] showed that when a suitable convention is chosen for locating the dividing plane, a specific surface excess free energy function can be defined, which equals the surface tension. Gibbs also gave a separate discussion of the stress induced by the surface in a solid, thereby anticipating the notion of the surface stress. Later Shuttleworth [50] showed that the surface stress of a planar solid surface can be described by a 2x2 tensor, **s**, defined in the plane of the surface. That definition relates **s** to the surface tension in a laboratory frame, and to the tangential strain tensor **e** by:

$$\mathbf{s} = \gamma \begin{pmatrix} 1 & 0 \\ 0 & 1 \end{pmatrix} + \frac{\mathrm{d}\gamma}{\mathrm{d}\mathbf{e}}. \qquad 2.1$$

Cahn [51] had outlined that the expression for the surface stress can be simplified by using the Lagrangian measure of the area. The relation between the Lagrangian area A_L and the physical area A is

$$A = A_L(1+e) \qquad 2.2$$

A_L is the surface area measured in a standard state of strain and remains unchanged during elastic deformation. Then, the Shuttleworth Eq.2.1 can be rewritten as:

$$\mathbf{s} = \frac{\mathrm{d}\gamma}{\mathrm{d}\mathbf{e}}, \qquad 2.3$$

a form which emphasizes that the entries of the surface stress tensor are independent thermodynamic parameters, which differs from the value of γ by magnitude and possibly sign. The two definitions yield the identical numerical value for **s**, but different functional dependencies of γ on the strain [52]. For a general surface it can be referred to a set of principal axes such that the off-diagonal components are identically zero. Furthermore, the diagonal components are equal for a surface possessing a three-fold or higher rotation axis symmetry. This means that the surface stress for a high symmetry surface is isotropic and can be measured by a scalar *f*, so the work for stretching the surface is *f*d*e*, with the scalar strain *e* defined as *e* = *trace* **e**.

$$f = \frac{d\gamma}{de} \qquad 2.4$$

The physical origin of the surface stress [26,24], from an atomistic point of view, can be understood in the way that at the surface of a solid the coordination of atoms is different from that inside of the bulk. Consequently, the charge density in the vicinity of the surface is redistributed. Correspondingly, the nature of the chemical bonding and the equilibrium interatomic distances at the surface are different from that inside the bulk. The surface atoms try to assume their equilibrium interatomic distances and that must be considered as exerting forces on the bulk, as long as the potential corrugation of the underlying atomic layer holds the topmost atoms on places of the bulk lattice.

2.2 Wafer bending technique for the measurements of the surface stress variation

While the experimental determination of the absolute surface stress remains a challenge, the experimental technique to measure changes in the surface stress is well established. The principles of the wafer bending method were first stated by Stoney [53], who derived an equation relating the stress changes in a thin layer to the radius changes of the curvature of the wafer. Measuring the bending of a plate to determine the stress in thin films is a common technique. One of the first experiments related to surface stress at the metal-electrolyte interface was performed by Gokhshtein [8] where the strain of the sample was produced by the fast potential pulses. Koch and Abermann [54], had measured the bending of the cantilevered wafer as the change of the gap of a capacitor using the three terminal capacitance methods [55]. Haiss [10,26] and Ibach [6] used electrochemical scanning tunnelling microscope (STM) to measure surface stress induced by potential at the metal-electrolyte interface. In their work a thin metal single crystal cantilever was used as the working electrode. STM tip monitored the surface stress changes induced by the electrochemical potential. Fredlein and Bockris [56, 57] first measured the potential-induced bending of a thin cantilever electrode by deflection of the beam of a laser using position sensitive detector. Later Floro and Chason [58, 59] significantly improved this method by passing the laser beam through a highly reflecting etalon that produce multiple output beams, thus providing multiple illumination of the sample. Use of multiple laser beams significantly reduces contribution of mechanical noises. So called multi optical stress sensor (MOSS) method is used in the current work for the measurements of the surface stress-charge coefficient in the nonadsorbing, highly diluted electrolytes.

2.3 Double layer, electrified interface

General information about the electrified metal-electrolyte interface is present in the next few paragraphs and mainly follows the Bard and Faulkner textbook [60]. Usually the electrochemistry field deals with the study of chemical changes caused by the passage of an electric current and the production of electrical energy by chemical reactions. In fact, the electrochemistry covers a huge array of different phenomena e.g. electrophoresis, corrosion and catalysis, devices such as electrochromic displays, electro analytical sensors, batteries and fuel cells, and technologies like the electroplating of metals, and the large-scale production of aluminium and chlorine.

Collections of interfaces are called electrochemical cells. These systems are defined most generally as two electrodes separated by at least one electrolyte phase. In general, a difference in electric potential can be measured between the electrodes in an electrochemical cell. It is a manifestation of the collected differences in electric potential between all of the various phases in the cell. The transition in electric potential in crossing from one conducting phase to another usually occurs almost entirely at the interface. The sharpness of the transition implies a very high electric field at the interface, and one can expect it to exert effects on the behaviour of charge carriers (electrons or ions) in the interfacial region. The magnitude of the potential difference at an interface affects energies of the carriers in the two phases. Thereby, the measurement and control of cell potential is one of the most important aspects of experimental electrochemistry.

By driving the electrode to more negative potentials (e.g. by connecting a battery or a power supply to the cell with its negative side attached to the working electrode), the energy of the electrons is raised (Figure 2.1a). The electrons can reach a level high enough to transfer into vacant electronic states on species in the electrolyte. In that case, a flow of electrons from an electrode to a solution (a reduction current) occurs (Figure 2.1a). Similarly, the energy of the electrons can be lowered by imposing a more positive potential, and at some point electrons on solutes in the electrolyte will find a more favourable energy on the electrode and will transfer there. Their flow, from solution to electrode, is an oxidation current (Figure 2.1b).

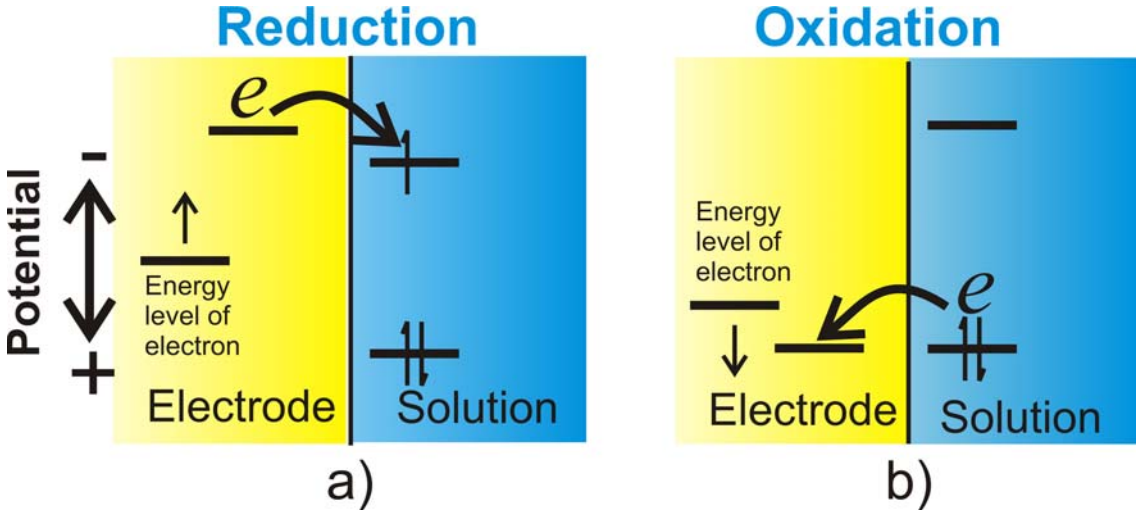

Figure 2.1. Schematic representation of a) reduction and b) oxidation process of a metal electrode.

2.3.1 Faradaic processes

At the electrodes occur two types of processes. One type is where the charges are transferred across the metal-electrolyte interface. Electron transfer causes oxidation or reduction to occur. Since such reaction is governed by Faraday's law (i.e., the amount of chemical reaction caused by the flow of current is proportional to the amount of electricity passed), they are called faradaic processes. Under some condition, a given electrode- solution interface will show a range of potentials where no charge-transfer occurs because such reaction is thermodynamically or kinetically unfavourable, for instance, between –0.5 and 1 V versus saturated calomel electrode (SCE) for a gold electrode in 0.1 M $HClO_4$(aq.). However, processes such as adsorption and desorption can occur, and the structure of the electrode-solution

interface can change with changing potential or solution composition. These processes are called nonfaradaic processes. Although a charge does not cross the interface, external current can flow when the potential, electrode area, or solution composition changes. Both faradaic and nonfaradaic processes occur when an electrode reaction takes place.

2.3.2 The ideal polarized electrode

An electrode at which no charge transfer can occur across the metal electrolyte interface, regardless of the potential imposed by an outside source of voltage, is called an ideal polarized electrode (IPE). While no real electrode can behave as an IPE over the whole potential range available in solution, some electrodes-solution systems can approach ideal polarizability over limited potential ranges.

For example, a mercury electrode in contact with a deaerated potassium chloride solution approaches the behaviour of an IPE over a potential range about 2 V. At sufficiently positive potentials the mercury can be oxidized in a charge-transfer reaction: $Hg+Cl^- \rightarrow ½Hg_2Cl_2+e$ at 0.25 vs natural hydrogen electrode (NHE), and at very negative potentials K^+ can be reduced $K^+ + e \rightarrow K(Hg)$, at –2.1 V vs NHE. In the potential range between these processes, charge transfer reactions are not significant. The water reduction is thermodynamically possible, but occurs at a very slow rate at the mercury surface

2.3.3 Electrical double layer

When the potential across the IPE interface is changed, the charge cannot cross it. This behaviour is analogous to that of a capacitor and governed by the equation:

$$q/E = C, \qquad 2.5$$

where C is the capacitance. The electrode-solution interface behaves like a capacitor. At a given potential a charge exist on the metal electrode, q^M, and in a solution, q^S. Depending on the potential across the interface and the composition of the solution the charge on the metal is negative or positive. However, q^M is always equal to $-q^S$. The charge on the metal represents an excess or a deficiency of electrons and resides in a skin layer (<0.1 A) on the metal surface. The charge in solution is made up of an excess of either anions or cations in the vicinity of the electrode surface. The whole array of charged species and oriented dipoles existing at the metal-electrolyte interface is called the electrical double layer (Figure 2.2). At a given potential, the electrode-solution interface is characterized by a double layer capacitance typically in the range of 10 to 40 μF/cm2.

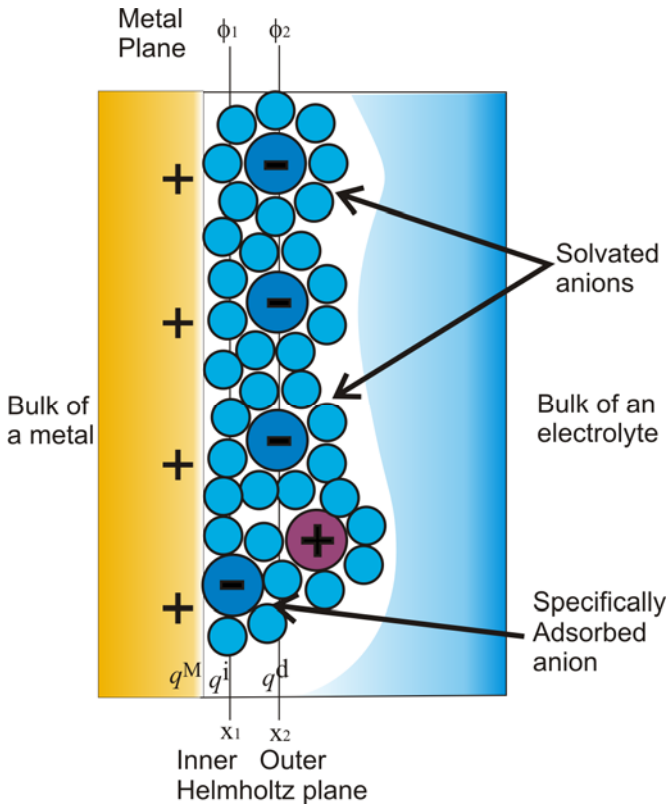

Figure 2.2 Model of the metal-electrolyte interface.

According to Gouy-Chapman theory [4,5], several layers can represent the solution side of the double layer. The inner layer, Figure 2.2, contains solvent molecules and sometimes other species (ions or molecules) that are specifically adsorbed. This inner layer is also called the compact, Helmholtz, or Stern layer. The position of the electrical centers of the specifically adsorbed ions is called the inner Helmholtz plane (IHP), which is at a distance x_1 from the surface. The total charge density from specifically adsorbed ions in this inner layer is q^i. Solvated ions can approach the metal only to a distance x_2; the position of centers of these nearest solvated ions is called the outer Helmholtz plane (OHP). The interaction of the solvated ions with the charged metal involves only long-range electrostatic forces, so that interaction is essentially independent of the chemical properties of the ions. These ions are said to be nonspecifically adsorbed. Because of thermal agitation in the solution, the nonspecifically adsorbed ions are also distributed in a three-dimensional region called the diffuse layer, which extends from the OHP into the bulk of the solution. The excess charge density in the diffuse layer is q^d, hence the total excess charge density on the solution side of the double layer, q^S, is given by:

$$q^S = q^i + q^d = -q^M. \qquad 2.6$$

2.3.4 Potential of zero charge

The potential of zero charge (pzc) is a fundamental property of the metal–electrolyte interface, and knowledge of this parameter is important for a detailed understanding of double-layer phenomena, electrochemical kinetics and the adsorption behavior of charged and neutral species [61,62]. The pzc is commonly defined as the potential, at which the electrode surface has no excess charge; for solid surfaces the *pzc* value can in many cases be obtained from double-layer capacity

measurements in dilute solutions, where a pronounced minimum appears at the pzc (Gouy–Chapman minimum) [60]. This has been demonstrated very nicely by the Meudon group for the three low-index faces of gold and silver single crystals [63,64].

2.4 Relation of the electrode potential to the work function

Establishing of the relation between the electrode potential and the work function, *W*, was a long standing problem in the electrochemistry [65]. This relation might provide a knowledge about the absolute value of the electrode potential. So far, the electrode potential in the electrochemistry is not an absolute value but always in the relation to some reference electrode. A common language, i.e., for understanding the structural relationship for the same system between the ultra high vacuum (UHV) and the electrochemical situation is needed. Up to now, the relation of the electrode potential to the absolute value is very controversial topic. This is because the parameter of the electrode potential, which is linked to the electron work function, is the potential of zero charge, *pzc*. The *pzc* could be determined only for very simple cases and even this can not be generalized yet. Ref. [65] is well representing the current status of this problem. At the same time, the relation between the changes of the electrode potential and the work function is easily determined by experiment. Rath and Kolb [47] combined the electrochemical method with the Kelvin probe microscopy and showed a linear one to one relation between the changes of the ΔE and ΔW (Figure 2.3). For the gold electrode the linear relation extends over a wide range of about 2 V.

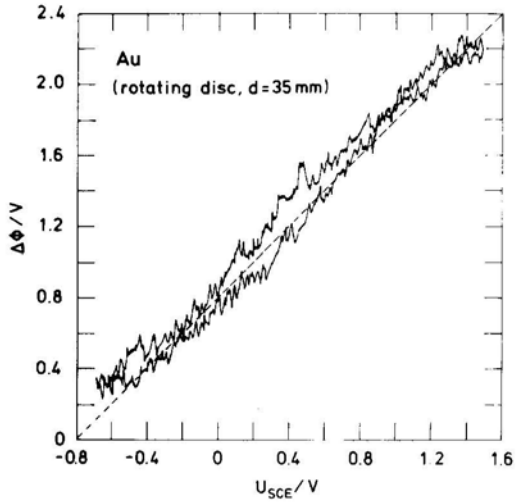

Figure 2.3. Work function of an immersed gold electrode as a function of emersion potential. 0.5 M $NaClO_4$. Scan rate 5 mV/s. Ref. [47]

3 Experimental procedure

3.1 Sample preparation

Two types of Au thin films samples were prepared. The substrate materials used for the deposition of Au are (100) silicon wafers or Kapton foils. The gold films deposited onto the polished surface of the (100) silicon wafers are used for the surface stress measurements in cantilever-bending experiments (Figure 3.1). The gold deposited on the Kapton foils are used for the measurements of electrode potential response to elastic strain using specially designed tensile machine (Figure 3.5).

3.1.1 Au on (100) silicon wafers

(100)-oriented silicon wafers of a nominal thickness of 100 μm and with a thermally grown, 100 nm thick oxide layer were obtained from CrysTec™ GmbH. Rectangular pieces of dimension (8×36) mm^2 were cut using a diamond cutter. Measurements of mass and area confirmed the thickness of the silicon wafers h = (100±2) μm. The gold metal film was deposited onto silicon surfaces using a thermal evaporation method in a vacuum chamber with a base pressure of 1×10^{-9} mbar. During the evaporation, the pressure was 1×10^{-8} mbar, with a deposition rate of 0.01 nm/s, controlled by a quartz microbalance, and a substrate temperature of 220 K. A titanium layer of about 2 nm thickness acts as a wetting layer. On top of the Ti layer, we evaporated Au to a thickness of 40 nm. These electrodes were prepared using facilities available at the Institute of Nanotechnology INT of the Forschungszentrum Karlsruhe in the group of Dr. Beckmann.

3.1.2 Au thin films on Kapton foil.

The substrate material used for the deposition of the Au thin film were polyimide (Kapton HN) films of dimensions (10 x 40) mm^2 and a thickness of 125 μm. A DC magnetron was used for the sample preparation. The chamber base pressure during the film deposition was $5x10^{-7}$ mbar. Gold films of 20 nm were deposited onto a 2 nm thick Ti supported Kapton film with a controlled deposition rate of 1.1 nm/s. Again, the Ti layer serves as a wetting layer for improving the sticking coefficient between the Au and the Kapton substrate. Prof. Herr at the University of Ulm provided the DC sputtering source facility.

3.2 Sample Characterization: X-ray, AFM

The X-ray diffraction was performed on the electrode specimens in reflection mode using a Panalytical X'Pert θ-θ diffractometer in Bragg-Brentano geometry with Ni-filtered Cu-K_α radiation and a position-sensitive solid-state detector.

The atomic force microscope (AFM) Nanoscope III was used to characterize the surface of the gold films deposited on silicon substrates. The AFM micrograph was made with a 1 Hz scan frequency in contact mode, force load 8.5 nN. The probe tip is a single crystal diamond (SCD) pyramid, which is mounted on a silicon cantilever,

was obtained from μ-mash™. The parameters of the probe are the following: the spring constant 0.15 N/m, the resonance frequency about 12 kHz, with aluminium coated backside. The measurements were carried out under ambient condition. A small piece of 1 by 1 cm^2 was cut prior to the measurement from the as prepared sample for the examination of the surface topology.

3.3 Experimental setup of the surface stress measurement combined with electrochemical setup

In solid electrodes, the surface stresses are generally coupled to the strain in the matter underlying the metal surfaces. Those strains can be determined experimentally e.g., by measuring the beam bending. In the present work, an optical method was employed to detect the bending of cantilevered wafers. A multi-beam optical stress sensor (MOS) system, k-Space™ [58,59] is capable of determining the surface stress variations during the bending movement of the cantilever with a higher precision then the optical system with the single beam.

As originally described by Stoney [53], stress in a thin film induces a curvature, k, in the substrate. The change in curvature is related to the surface stress by the well-known Stoney equation:

$$k - k_0 = \frac{6f}{M_s h_s^2}, \tag{3.1}$$

where k_0 is the initial curvature of the unstressed substrate. The other parameters in this equation are the biaxial modulus of the substrate, M_s, and the substrate thickness, h_s. The biaxial modulus of the film is related to the bulk modulus, Y, by the Poisson ratio, ν:

$$M_s = \frac{Y}{1-\nu}. \tag{3.2}$$

The key to the stress measurement is therefore obtaining a precise measurement of the curvature. A sketch of the MOS apparatus for measuring the sample curvature optically is shown in Figure 3.1. In this approach, an array of parallel laser beams illuminates the electrode surfaces. The actual measurement consists of the determination of the spacing of the beams reflected from the surface when they reach the face of the charge-coupled device (CCD) camera. If the surface is flat, then the beams will have the same spacing after reflection as they had in the incident beam array. If the flat surface starts to bend, the laser beams deflect under different angles and the spacing of the beams on the CCD changes.

The change in the spacing of the reflected beams, monitored using a CCD camera, is a direct measure of the stress-induced curvature of the electrodes. As shown in the figure 3.1b; the curvature change induced by the stress is related to the spacing of the deflected beams by:

$$k - k_0 = \left(\frac{\delta d}{d_0}\right)\frac{\cos\alpha}{2L} \tag{3.3}$$

δd is the difference in the beam spacing from the initial spacing, d_0, due to the stress-induced curvature. The ratio $\delta d/d_0$ is referred to as the differential spacing. The distance of the sample from the camera is L and the angle between the beam array and the sample normal is α. Combining this measurement with the Stoney formula [53]

shows that the measured surface stress is directly proportional to the measured spacing of the deflected beams, as given by:

$$\Delta f = \left(\frac{\delta d}{d_0}\right)\frac{M_s h_s^2}{12L}\cos\alpha\,, \qquad 3.4$$

This generalized Stoney's equation is used for calculation of the surface stress of a thin film using the MOS system.

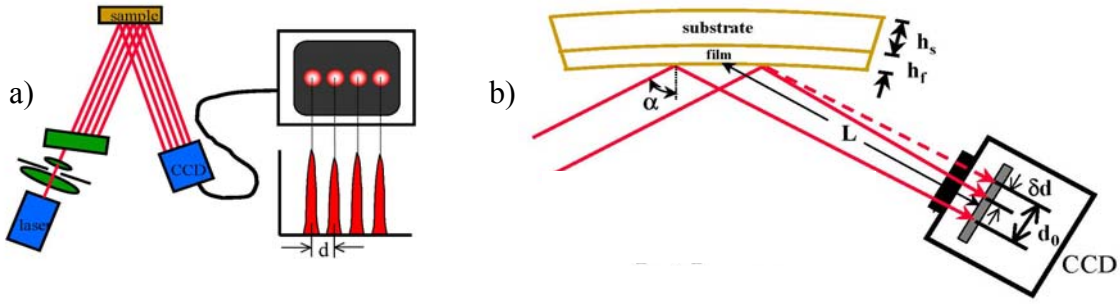

Figure 3.1 a) The MOS system uses an array of parallel beams to illuminate the sample. The position of the beams is measured with a CCD camera. A framegrabber digitizes the image and the MOS software calculates the beam spacing, *d*. b) Stress in thin films induces curvature in the substrate. The MOS system measures the curvature optically by monitoring the deflection of parallel beams of light

3.3.1 Surface stress measurements at the metal-electrolyte interface

The curvature changes of the (111) textured gold film were measured in-situ by MOS system in response to the electrochemical surface charging. The sample was immersed into the electrochemical cell (3 in Figure 3.2) as the working electrode (WE in Figure 3.2). The surface of the sample was illuminated by the He-Ne laser (1 in Figure 3.2) by an array of 4×4 or 3×3 parallel laser beams (Figure 3.2b).. The distance, *L*, from the sample to CCD device (8 in Figure 3.2) was *L*=107 cm with inclination angle $\alpha = 3°$.

The primary data from the curvature analysis were two time-dependent values for the differential spot spacing, $\Delta d/d_0$, measured along two orthogonal directions ('*x*' and '*y*' in Figure 3.2b). The spot spacing relates to changes in the resolved curvature along the respective direction, parallel to the long (curvature κ_y) and short (κ_x) axis of the cantilever, respectively. The laser passes through three different media, air, glass and aqueous electrolyte. Because of that, it is necessary to account for a refractivity index of the aqueous electrolyte. The solvent refractivity index *n*, was taken as for water, 1.33. Due to the low concentration of NaF and $HClO_4$ in the aqueous solution, this is a valid assumption. Therefore, in the Eq. 3.4, the electrolyte refractivity index have to be included. Finally, in this work the surface stress was calculated using the following formula:

$$\Delta f = \left(\frac{\delta d}{d_0}\right)\frac{M_s h_s^2}{12Ln}\cos\alpha\,. \qquad 3.5$$

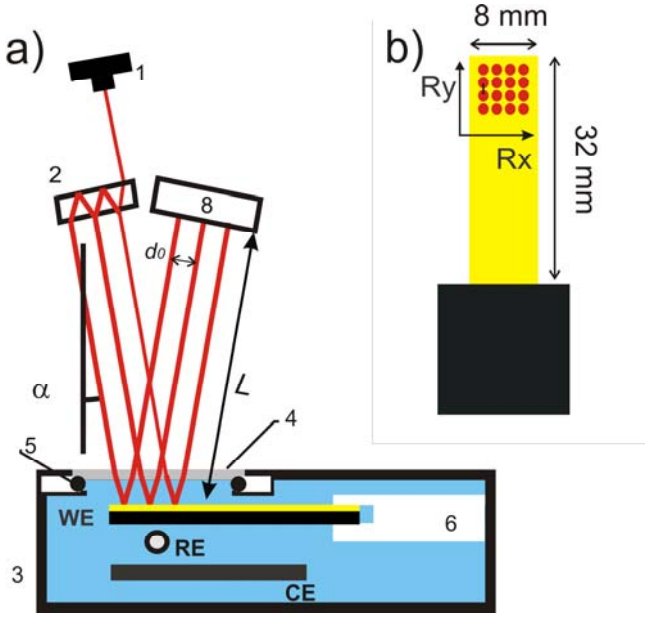

Figure 3.2 The cantilever-bending experimental setup of: a) Schematic illustration of the experimental set-up. Teflon made electrochemical cell: Cantilevered working electrode (WE) made from 100 μm (100) Silicon wafer with 40 nm evaporated gold gently fixed at one end and immersed into the electrolyte. The reference electrode (RE) SCE connected to the cell through lugging capillary. A gold plate was used as the counter electrode (CE). The cell was sealed using an optically transparent glass plate and a teflon coated O-ring. The laser path: 1 He-Ne laser; 2 *x*- and *y*- optical etalons; 3 electrochemical cell; 4 glass; 5 teflon coated O-ring; 6 wafer holder clamps; 8 CCD camera; α-angle between incident beam and sample surface, *L* sample-CCD camera distance, d_0 distance between laser spots reflected from the WE; b) Illustration of the two bending radii, R_x and R_y.

The laser path from the sample to the CCD camera was measured using mirrors with known radii of curvature (10 m and infinite for the planar one). It was calibrated as (107±3) cm.

When the electrode potential is changing, then the surface stress tensor, **s**, at the electrode surface varies and the compensating stress in the cantilever gives rise to bending. By symmetry, **s** must be isotropic on 111-oriented surfaces of fcc crystals, so that we can identify each of the resolved values **s** with the scalar surface stress value as $f = ½trace\ \mathbf{s}$. The derivation of Stoney's equation for biaxial bending makes use of the classical lamination theory. The lamination theory requires that the normal displacements are much less than the beam thickness. Here, this requires $kb^2 \ll h$, where b is the dimension of the cantilever orthogonal to the bending direction. In the present experiments, the maximum curvature change corresponded to the smallest radii around 500 m. With b = 8 and 36 mm, the condition was well satisfied for bending along both directions.

The values of Young's modulus, Y = 130.2 GPa, and Poisson's ratio, v = 0.279 of 100-oriented Si as given in [66]. Applying Eq. 3.5 separately to each of the two

experimental curvature values κ_x and κ_y and solving for f provides two independent measurements for the nominally identical quantity f.

The experimental error in f may be estimated as follows: The uncertainties quoted above for h_S, L and α add up to a systematic uncertainty of around 7%. The statistical experimental uncertainty – as estimated from the scatter in individual measurements –was about 1%. It was found, the apparently largest source of possible systematic error arises from the partial suppression of the transverse bending due to constraints from clamping. To minimize this effect, the laser spot array probed the curvature near the free end of the cantilever, about 2.6 cm or three times the wafer width, from the clamp. According to Ref. [67], free biaxial bending is expected as long as the distance is larger than the wafer width. Nevertheless, a noticeable anisotropy in the curvature was found, and the surface stress value inferred from the transverse bending component was less than the longitudinal one by about 10%. Since, as it was discussed before in this section, the symmetry requires **s** to be isotropic, the result suggests that noticeable clamping effect remains. The longitudinal curvature component and the surface stress value determined from it are not affected by clamping, that component was selected as more reliable and was used for quantitative analysis.

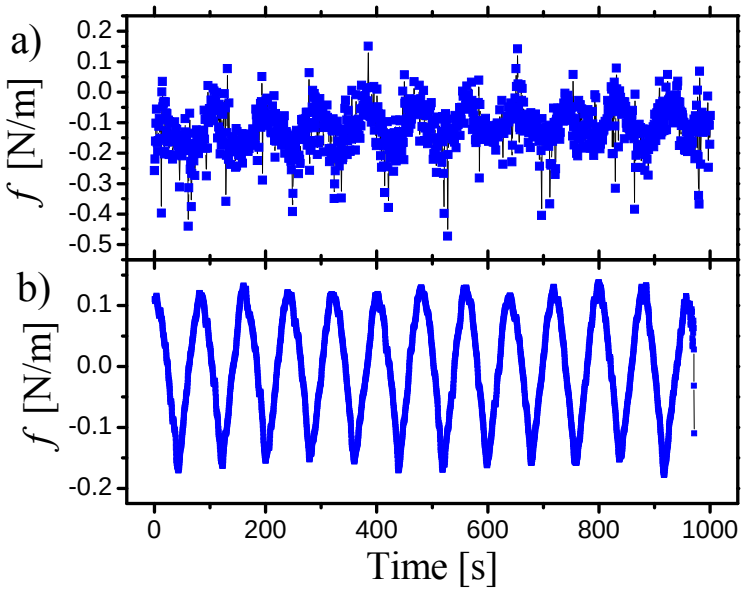

Figure 3.3 The surface stress of a (111) textured Au in 7 mM NaF measured with a laser path between the electrochemical cell and the optics unit: a) open to the air; b) housed in a plastic tube**.**

It was also found that a significantly improved signal to noise ratio could be obtained when air convection in the (vertical) laser path was suppressed by inserting a plastic tube between the electrochemical cell and the optics unit. The surface stress measurement without and with a housed vertical laser path are shown in Figure 3.3.

3.3.2 The electrochemical cell

Prior to the experiment, the electrochemical cell was placed in the standard cleaning solution (5 volume parts of conc. H_2SO_4(aq.) + 1 part of 30% H_2O_2(aq.)) for

24 hours and then rinsed thoroughly with ultrapure 18.2 MΩ cm grade water (Arium 611, Sartorius). The same water, plus $HClO_4$ (Suprapur®, Merck) or NaF (Suprapur®, Merck), were used to prepare the aqueous electrolytes. All cyclic voltammetry was performed with a PGSTAT 10 potentiostat (Eco Chemie); the charge transfer to the electrode was computed by integrating the current, using the potentiostat's 'current integration' mode.

The rectangular cell of about 150 ml capacity, made of electronics grade Teflon, contained the horizontal cantilever as the working electrode and a coplanar gold plate with a surface area of 10 cm^2 as the counter electrode. A saturated calomel electrode (SCE) as reference electrode was connected to the cell through a Teflon Luggin capillary and sealed with a Teflon coated O-ring. In the interest of charging kinetics and low uncompensated resistance between reference and working electrodes it would be desirable to arrange the Au-coated side of the sample down, facing the counter electrode. However, the low reflectivity of the back side of the sample prevented a meaningful evaluation of the reflected laser beams in this configuration; the cantilever was therefore arranged with the Au film (which had good reflectivity) facing up. The cell was filled with electrolyte completely, so that the cantilever was wetted on all sides, and a glass plate sealed with a Teflon-coated O-ring closed the cell.

The active Au surface area for different samples varied between 2.4 cm^2 and 2.9 cm^2. To further diminish mechanical constraints, the clamp was tightened with the minimum force required to fix the wafer. Screws and clamp were made of Teflon. The electrical contact with the thin film was provided by a thin (~100 μm diameter) gold wire.

3.3.3 Experimental measurement potential of zero charge at metal-electrolyte interface

The potential of zero charge (*pzc*) was determined from the potential-dependent capacitance curve for an as prepared film sample. The differential capacitance was measured at the frequency of 18 Hz and the amplitude of 10 mV of ac potential. The contact between the sample and electrolyte was arranged by means of the hanging meniscus method [68]. An Ag/AgCl capillary electrode in saturated KCl(aq) was used as the reference electrode. Later the potential was converted to the saturated calomel electrode (SCE) as the reference.

3.4 Experimental methods of the electrode potential response to an elastic strain measurement

This section describes the alternative experimental approach used to verify the thermodynamic Maxwell relation (Eq. 1.2). In this approach, the electrode potential was measured as the function of the elastic strain of the metal electrodes. Two experimental techniques were used. A balance method, similar with Horvath and Schiller approach [45], was used as an initial stage. In the balance method, the electrode potential measured at the time when the elastic strain applied to a metal wire. The second approach was developed during the thesis project. In this approach the cyclic elastic tension was applied to the metal film. The Correspondent electrode potential response was measured using the Lock-in technique.

In the case of metallic solids, the reported surface stress-charge coefficient values, $\varsigma = \mathrm{d}f/\mathrm{d}q$, is about of –0.9 V [10]. From the Maxwell relation, eq. 1.2, the expected value of ΔE produced by the elastic strain e (typically less than 0.2 %) is in the range of 200-600 μV. This is just above the potentiostat resolution used for measuring the electrode potentials. More precisely, the measurement accuracy is +/– 30 μV, for the case, when the potential difference between working and reference electrodes or potential measuring scale are below 100 mV. It was mandatory to measure the electrode potential-elastic strain response at the conditions of a constant charge. It is realized if the potentiostat set to open circuit potential, *ocp*. The open circuit potential is the condition at which no current flows from the working to the counter electrode and it is equivalent to the constant charge at the working electrode. The typical *ocp* value for the Au electrode is 300 mV versus Ag/AgCl. The best potentiostat resolution in that case is 300 μV. This is not enough to resolve the signal. The accuracy of the measurements is possible to improve using identical metal for reference and working electrodes. The *ocp* value across two identical electrodes is zero. Unfortunately, the potential difference also would be zero for special cases. For instance, two identical electrodes are oxide covered and they are in the same oxidation state or contaminated with adsorbed atoms of the same chemical elements. These aspects make it difficult to define the electrode surface state. That may lead to ambiguous errors in experimental results, especially the sign and amplitude of the potential signals. Therefore, it is a good practice not to use identical working and reference electrodes for this type of experiments. If identical electrodes are used, then it is important to pay attention on their surface chemical purity.

It is more reasonable to use non-polarisable and ideally reversible reference electrodes; Ag/AgCl in KCl(aq.) is an example. The *ocp* value for Au is in the range from 200 to 300 mV versus Ag/AgCl. At this potential range, the resolution of the instrument (potentiostat) is +/- 300 μV. This value is also very close to the expected variations of the electrode potential, ΔE, in response to the elastic strain, Δe. Therefore, an accurate determination of ΔE during reversible straining is quite difficult.

The new experimental method was developed to measure the effect of the elastic strain on the potential of an electrode. The experimental setup including a tension apparatus for generating cyclic elastic strain and an experimental infrastructure for the measurement of change in electrode potentials, ΔE, was designed. In the tension apparatus, the piezo-actuator cyclically strains the working

electrode within a frequency range between 0.2 Hz and 100 Hz. The preliminary experimental results were obtained using the balance method. The working principles of the method described in the next paragraph.

3.4.1 Experimental setup for measurements of potential-elastic strain response of a metal wire: Balance method

The measurement technique is based on the principle of a mechanical balance, that principle gives the name to the method. Figure 3.4 shows the schematic working assembly of this setup. A metal wire as the working electrode immersed into the electrolyte is attached to the balance. The external load applied to the other end of the balance arm creates a tensile mechanical deformation to the wire. The potential difference during the loading and unloading events is the measure of change in electrode potential ΔE due to the mechanical stress.

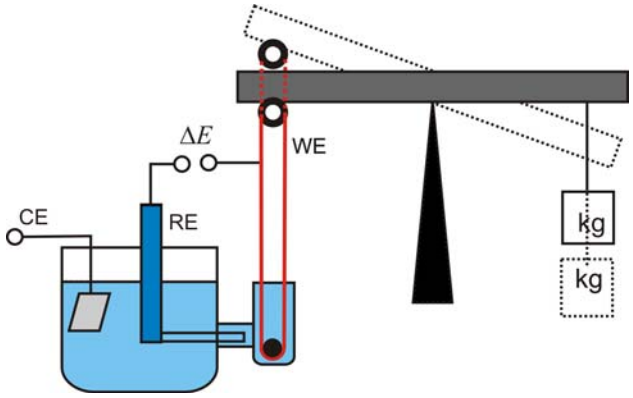

Figure 3.4 The balance method. Open circuit potential, ΔE, measurements of a strained wire in an aqueous electrolyte. WE, RE, CE – working, reference and counter electrodes.

The working, reference and counter electrodes were electronic grade Pt wire of 0.25 mm diameter, obtained from Goodfellow. The aqueous solution of 0.1 M H_2SO_4(aq.) was used as an electrolyte. During the measurement, the cell was continuously purged with ultrapure Ar gas. A potentiostat measured the change in potential between the working and reference electrodes. A set of standard weights in the range of 5 to 100 g were used for the loading and unloading events created the mechanical stress to the electrodes.

Because of uncertainties in the amplitude of applied strain and a high risk of having plastic deformation of the wire it was desirable to find another way to study the effect of an elastic strain on the electrode potential. The new method developed by the author is described in the next paragraph.

3.4.2 Experimantal concept for the measurements of the potential-elastic strain response of a metal film

Herr and co-workers [69] reported an elastic strain amplitude of up to 1% for 20 nm thick cobalt sputtered on a polyimide substrate (Kapton). Based on this property of thin metals attached to elastic substrate and our in-house experience acquired from the balance method the new tension setup for the measuring of the

electrode potential variation in respect to the cyclic elastic strain was developed, a schematic view is shown in the Figure 3.5. A piezo-actuator with capacitive strain gauge is used for the application of a cyclic elastic strain to the sample. The function generator (9 in the Figure 3.5) connected to the control unit of the piezo-actuator (8 in the Figure 3.5) controls the linear mechanical motion of the piezo-actuator (7 in the Figure 3.5). Build in the piezo-actuator the capacitive strain gauge measured the actual periodical displacement of the piezo-element which was rigidly attached to the sample. The piezo-actuator assembly strained the sample with high precision at different driving frequencies up to 100 Hz. A lock-in amplifier (5 in the Figure 3.5) detected the potential response of the metal electrode (1 in the Figure 3.5) to the elastic strain at the reference frequency of the piezo oscillation. The assembly presented here allows:

i) Applying the cycling elastic strain to the metal film of the amplitude in the order of 10^{-5}.

ii) The amplitude of the potential response, which explicitly corresponds to the applied cyclic elastic strain, was measured with a high precision using the lock-in technique.

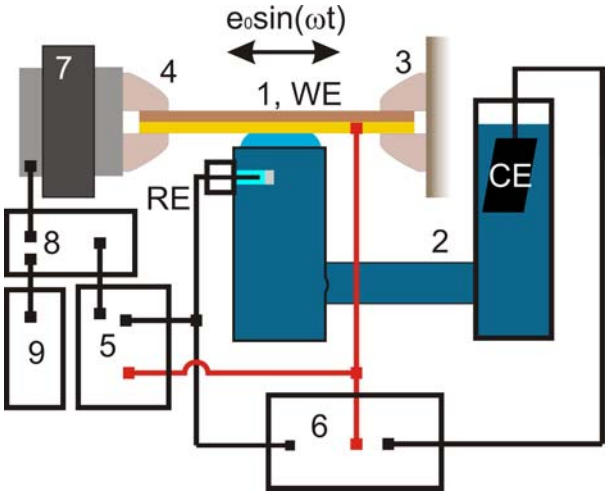

Figure 3.5 Schematic view of the experimental setup for the measurements of $dE/de|_q$: 1 – the sample, working electrode, 2 – electrochemical cell contained aqueous electrolyte; 3 – stationary sample clamps; 4 – sample clamp connected to the piezoactuator,7; 5 – Lock-In amplifier connected in parallel to the RE and WE electrodes; 6 – potentiostate; RE, WE, CE – reference, working and counter electrodes respectively; 7 – piezoactuator; 8 – piezoactuator control unit; 9 – function generator.

3.4.3 Mechanical arrangements of the cyclic elastic strain

Figure 3.6 represents the top and side views of the in-house built tension apparatus for the measurement of the electrode potential variation. Photographs of the experimental setup are shown in Figure 3.7 and Figure 3.8. The thin Au film on Kapton is the working electrode (label 1 in Figure 3.6). The corrosion resistive grips (labels 2a and 2 b in Figure 3.6), made of Peak® material, fixed the working electrode at the both ends. The gauge (label 2a in Figure 3.6) holds the working electrode in a fixed position. The grip (label 2b in Figure 3.6) is connected to a piezoactuator device (label 4a of Figure 3.6) through an assembly of a metal slider (label 5 in Figure 3.6) in a

cylindrical housing (label 4a in Figure 3.6). This part (label 4a in Figure 3.6) controls the horizontal positioning of the electrode–piezo assembly. The metal slider (label 5 in Figure 3.6) moves back and forth with respect to the main stage (label 6 in Figure 3.6) using a threaded rod. The slide was fixed in its final position by head screws (label 7 in Figure 3.6). Finally, a stainless steal metal platform (label 6 in Figure 3.6) supports the electrochemical cell (label 3 in Figure 3.6), the piezo-device and their accessories.

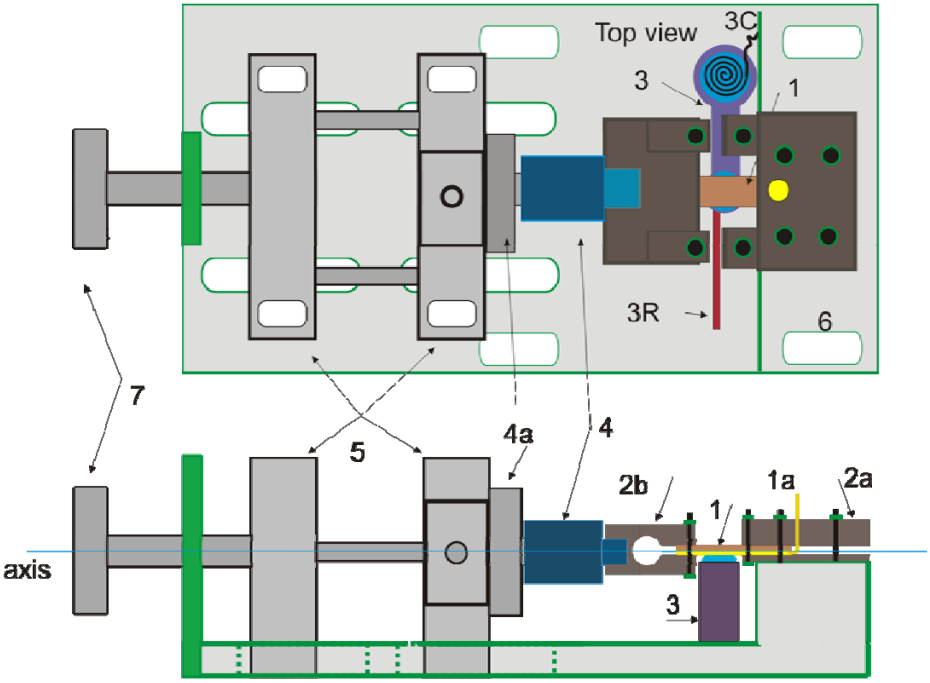

Figure 3.6 Top and side views of mechanical setup of tension machine. 1 – the sample, 2 – sample grip, 3 – electrochemical cell, 3R and 3C – position of reference and counter electrodes, 4 – piezoactuator, 5 – holder of piezoactuator, 6 – stainless steal support, 7 – screw for adjust to the sample length.

3.4.4 Sample mounting into the tension apparatus

The experimental arrangements were performed in the following steps. The grips (labels 2a,b in Figure 3.6) hold the working electrode during the mechanical straining. The Au deposited side of the Kapton substrate was placed downwards and wetted from below. A thin Au wire (label 1a in Figure 3.6) connected to the metal side of the sample served as an electrical connector. An electrochemical cell (label 3 in Figure 3.6, see for more details Figure 3.9), made of a high purity Teflon was used in the experiment. The cell contains two cylindrical shaped compartments (label 3 in Figure 3.6 top view) for counter electrode (label 3C in Figure 3.6) and the reference electrode (label 3R in Figure 3.6) which was placed under the working electrode surface in a fixed position. A cylindrical tube connects the counter electrode compartment with the working electrode compartment.

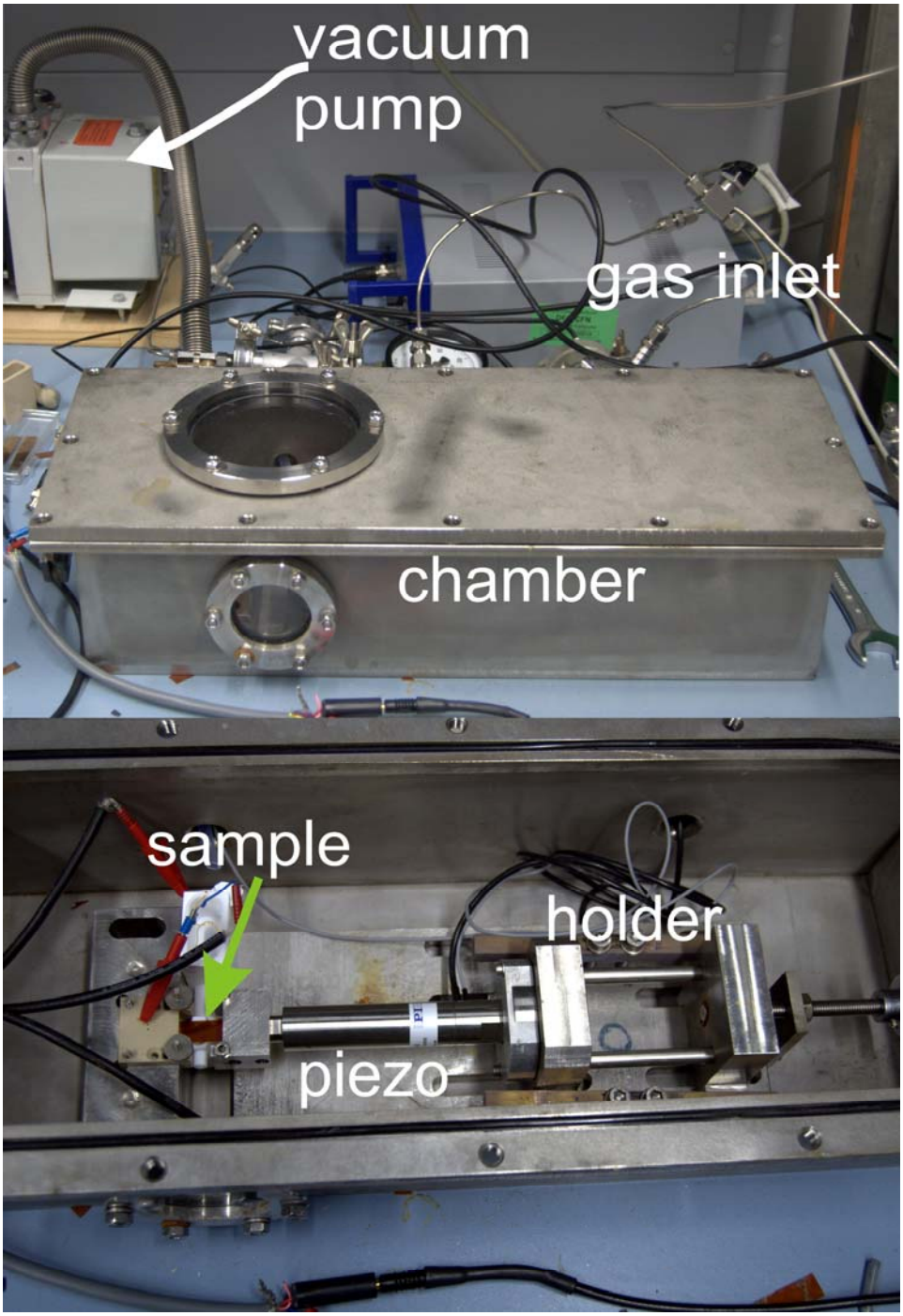

Figure 3.7 Experimental setup. Upper photograph: the vacuum chamber built for the potential-strain experiment. Lower photograph: the experimental arrangements - the tension apparatus with the sample and the electrochemical cell.

It was important to avoid buckling of the sample during the experiment. The micro screw adjuster (label 7 in Figure 3.6) was used to minimize the buckling effect by prestraining the sample after the mounting procedure. This part (label 5 in Figure 3.6) was tightened by screw on the metal platform (label 6 of Figure 3.6) for mechanical rigidity after optimizing the ideal working position of the electrode.

3.4.5 The inert gas chamber

The measurements were done in an inert gas atmosphere. The chamber was made of a stainless steel, containing three KF16 vacuum feedthroughs and two glass windows (Figure 3.7). The vacuum feedthroughs are used for electrical connections (a potentiostat to the cell and a piezo-control unit to the piezoelement) and pipelines for a gas and a vacuum pump.

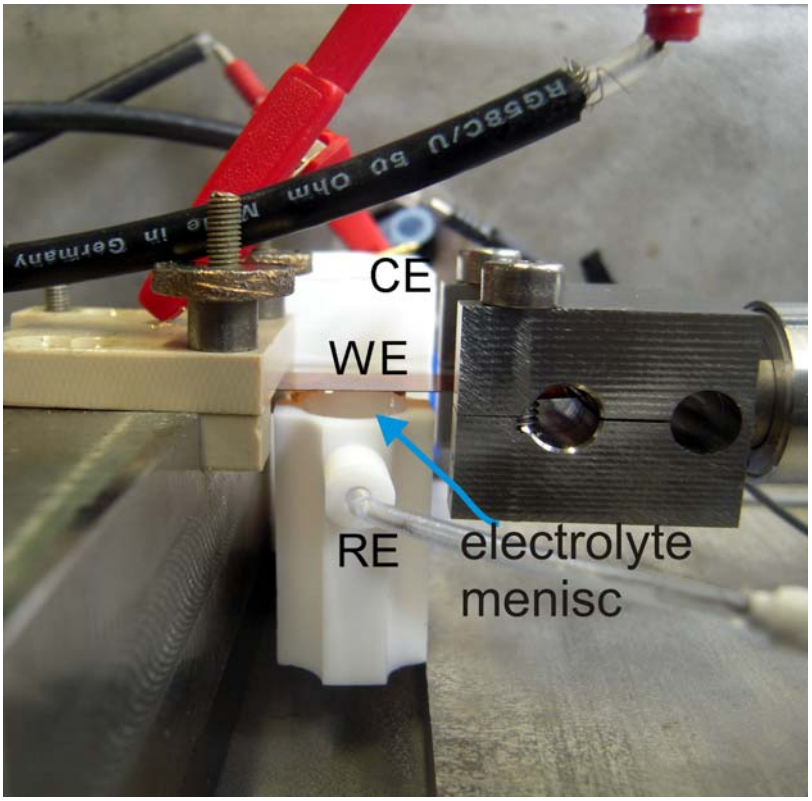

Figure 3.8 Photograph of the experimental set-up. The sample, Kapton foil with a 20 nm gold film – working electrode (WE), is mounted between two clamps; the piezo-actuator is connected to the titan clamp. A teflon cell is placed below the sample. The cell filled the aqueous electrolyte till the meniscus contact formed with the gold covered side of the sample. Positions of the reference and counter electrodes depicted as RE and CE respectively.

3.4.6 Installation the sample into the tension apparatus

The tension apparatus was placed into a vacuum chamber, Figure 3.7, with the electrochemical assembly. The electrochemical cell was filled with the aqueous electrolyte till the liquid contacted the gold covered side of sample (Figure 3.8). The chamber was pumped until the 500 mbar pressure, then the Argon gas was purged into the chamber. Important was to maintain the chamber pressure not less than 500 mbar, otherwise the liquid in the reference electrode leaked from the capillary tube. The chamber was flushed several times with Argon gas and than pressure inside was set to 1000 mbar.

The electrochemical-strain set-up consisted of a GAMRY and AUTOLAB PGSTAT 10 potentiostates, a digital lock-in amplifier (Stanford Research 830), a

Physical Instrument P-845.40 piezodriver with capacitive stress gauge, a Physical Instrument E-665.XR piezodriver control unit, and a TG–315 function generator. The analogue outputs of the lock-in and the stress gauge were digitized and transferred to a personal computer by an analog-digital USB converter (Measurement Computing).

3.4.7 Measurement of electrode potential-elastic strain response

The experiment starts with cyclic voltammogram (CV) measurements. During this procedure, the electrode potential changed linearly. It caused the electrical current pass through the metal-electrolyte interface. After several CVs in the double layer interval the electrode potential is stopped at the value close to the *pzc*. The control over the electrochemical cell is turned off. At this condition, the current between the counter and the working electrodes is zero. The electrochemical cell is at open circuit potential. After the equilibrium condition was reached, the cyclic elastic strain was applied to the working electrode. The open circuit potential (E_{oc}), as the function of the elastic strain, was measured.

As mentioned before, the piezo-actuator has build in capacitive strain gauge which measure the actual displacement of the sample ΔL. The areal strain of the gold deposited on the Kapton foil was calculated using following expression:

$$\varepsilon = (1 - \nu_K)\frac{\Delta L}{L} \tag{3.6}$$

where L denotes the sample length and ν_K the Poisson ratio of the Kapton, equal to 0.35 [70].

4 Results

4.1 Microstructure of the gold electrodes

Figure 4.1 shows the results of the surface characterization of an as-prepared gold film evaporated onto a (100) silicon substrate made by atomic force microscope (AFM). From this image the ratio between projected, A_p, and real, A, surface area was calculated using the v700 software (NanoScope). It gives a roughness factor of the gold film, A/A_p, about 1.1. The image suggests a characteristic lateral feature size of islands on the Au surface around 80 nm. The surface height profile standard deviation is 3 nm. Thus, gradients of height appear small. An extended discussion about the role of the surface roughness for the measured surface stress can be found in the report of Weissmüller and Duan [33]. The influence of the surface roughness on the surface stress of the present experiment is discussed in details in chapter 5.1.5.

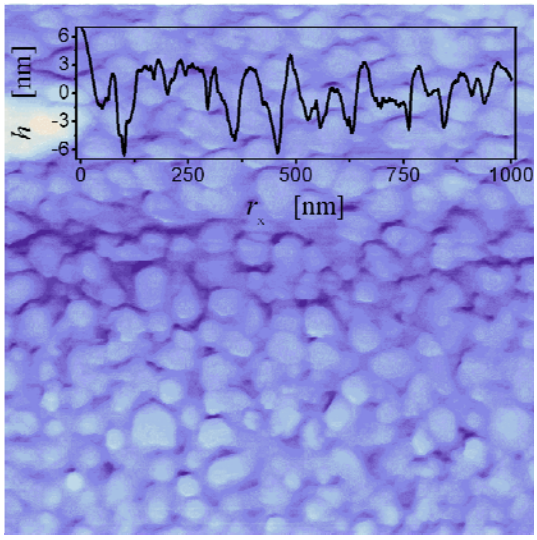

Figure 4.1. AFM micrograph of a 1×1 μm^2 area of working electrode surface in the as prepared state. The insert shows height h versus position r_x on a characteristic cross-section.

The crystallographic features of the gold films was investigated by X-ray diffraction. The (200) reflection was absent in θ-θ X-ray scans (Figure 4.2), indicating a (111) crystallographic texture. This is confirmed by the rocking curves for the (111) reflection which yield a full-width at half-maximum of 3.2° for the gold film on the silicon substrate and 12° for the gold film on the Kapton (insets in Figure 4.2),. Summarizing the AFM and X-ray data the surface may be qualified as smooth and preferentially (111) oriented.

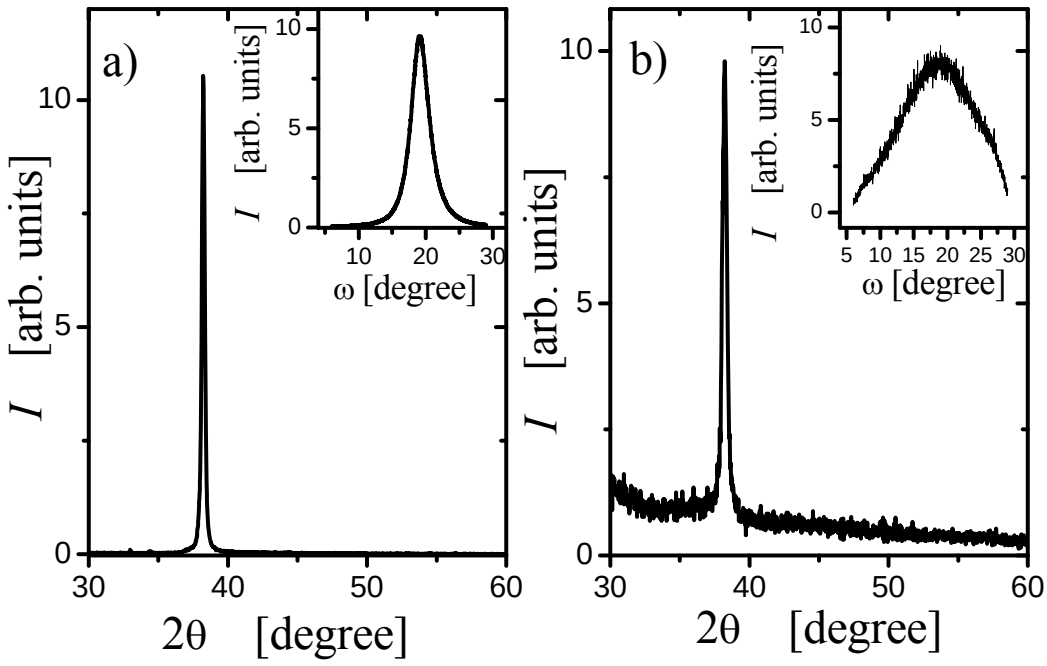

Figure 4.2 X-ray characterization of the Au electrode. Main graph: Intensity *I* versus scattering angle 2θ. Inset: Rocking curve of *I* versus inclination angle ν for the (111) reflection, (a) of 50 nm Au films on a (100) Si substrate; (b) of a 20 nm Au film on a Kapton substrate.

4.2 Potential of zero charge of the (111)-textured gold electrode in aqueous solutions of NaF and $HClO_4$

A further important property of the metal-electrolyte interface is the potential of zero charge (*pzc*). Figure 4.3 shows the differential capacitance curves of a 50 nm Au film on a gold substrate measured in aqueous solutions of 7 mM NaF(aq.) and of 10 mM $HClO_4$(aq.). The differential capacitance was measured after several potential cycles. The two curves (Figure 4.3) exhibit a pronounced minimum, which is attributed to the *pzc*. A quadratic fit in the vicinity of the capacitance minimum yields E_{zc} = (180±10) mV for the case of NaF(aq.) and E_{zc} = (200±10) mV for $HClO_4$(aq.). This is in good agreement with values reported in the literature, namely 230 mV for a bulk-terminated gold single crystal in 0.01 M $HClO_4$(aq.) [71]. The *pzc* of reconstructed Au(111)-($\sqrt{3} \times 22$) is considerably more positive, 320 mV versus SCE both in 0.01 M $HClO_4$(aq.) [71] and in 0.01 M NaF(aq.) [78]. The comparatively negative value found here suggests that the surface of the present Au films was bulk terminated.

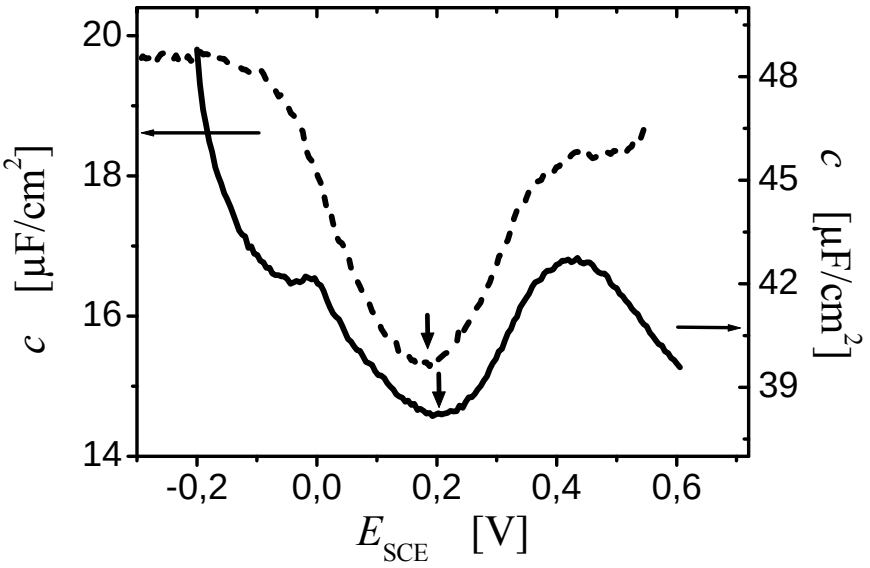

Figure 4.3 Differential capacitance vs. potential for (111)-textured Au in 7 mM NaF(aq.) (dashed line, left axis) and 10 mM $HClO_4$(aq) (dotted line, right axis). The arrows denote the potential of zero charge which is (0.18±0.01) V in aqueous NaF and (0.20±0.01) V in $HClO_4$.

4.3 Surface stress of (111) textured Au film in diluted aqueous electrolytes

4.3.1 Anisotropic aspects in the detection of the wafer bending

A sample bending was measured in two orthogonal directions. A representative graph of the time-dependent differential spot spacing, $\delta d/d_0$, during the cyclic variation of the electrode potential, E, is shown in Figure 4.4 . One can see that $\delta d/d_0$ varies reproducibly in phase with the electrode potential, and that the signal-to-noise ratio is excellent. The two curves of $\delta d/d_0$ represent the results for the two orthogonal bending directions. A slight difference between the longitudinal and transverse directions is visible in the Figure 4.4. The reduced amplitude in the transverse direction, as discussed in the paragraph 3.3.1, is due the constraints occur from the sample clamping. Therefore, the longitudinal $\delta d/d_0$ signal is used in the data analysis for the surface stress evaluation.

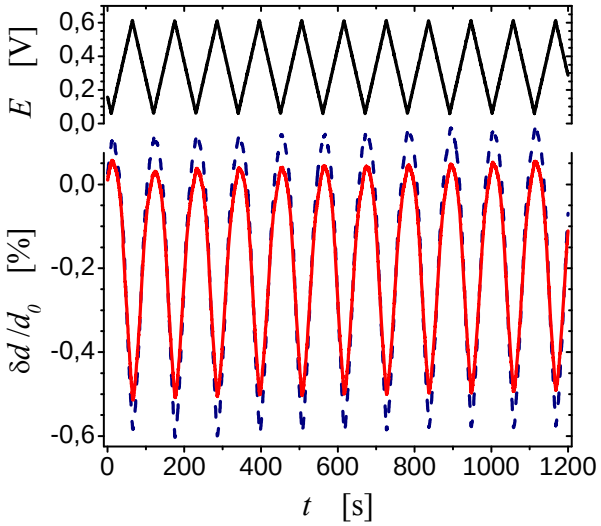

Figure 4.4. Electrode potential, E, (top part of figure) and variation of the differential spot spacing, $\delta d/d_0$, (bottom part) represented as the function of time, t, (during eleven successive voltammograms in aqueous solution of 10 mM $HClO_4$). The curves in the bottom part scales with the changes of curvature of the wafer in longitudinal (blue, dotted) and transverse (red, solid) direction (compare Figure 3.2).

4.3.2 Experimental measurements of the surface stress of (111)-textured gold electrode in aqueous solution of NaF

The wafer bending technique was used for measuring the surface stress of the metal during electrochemical charging in aqueous electrolytes. In-situ surface stress, Δf, measurements of 50 nm thick (111)-textured gold film deposited on the silicon substrate were carried out in 7 mM NaF(aq.) at 10 mV/s scan rate and in a potential range of 0.4 V centered near the *pzc*. Figure 4.5, displays the current density, j, the charge density change, Δq, and the surface stress change versus the electrode potential, E. The cyclic voltammogram (CV) of (Figure 4.5a) shows a featureless behaviour, indicating the dominance of double layer charging in the metal-electrolyte interface. The curve of the charge density (Figure 4.5b) is closed, indicating that in the system the charge is conserved. Figure 4.5c shows the change in the surface stress versus electrode potential. The surface stress was recorded for more then ten cycles of the electrode potential. Note the noticeable hysteresis and the good reproducibility the surface stress data. The key graph is the Figure 4.5d. This figure displays a curve of the surface stress versus the charge density. One could see from there that the relation between Δf and Δq is linear with negative slope. A linear regression of the graph of $f(q)$ gives the surface stress-charge coefficient $\varsigma = (-1.95 \pm 0.01)$ V. For the first time the value of ς measured in non-adsorbing highly diluted aqueous electrolyte. The number is in perfect agreement with the theoretically obtained results for the charged metal in vacuum, which was –1.89 V [11].

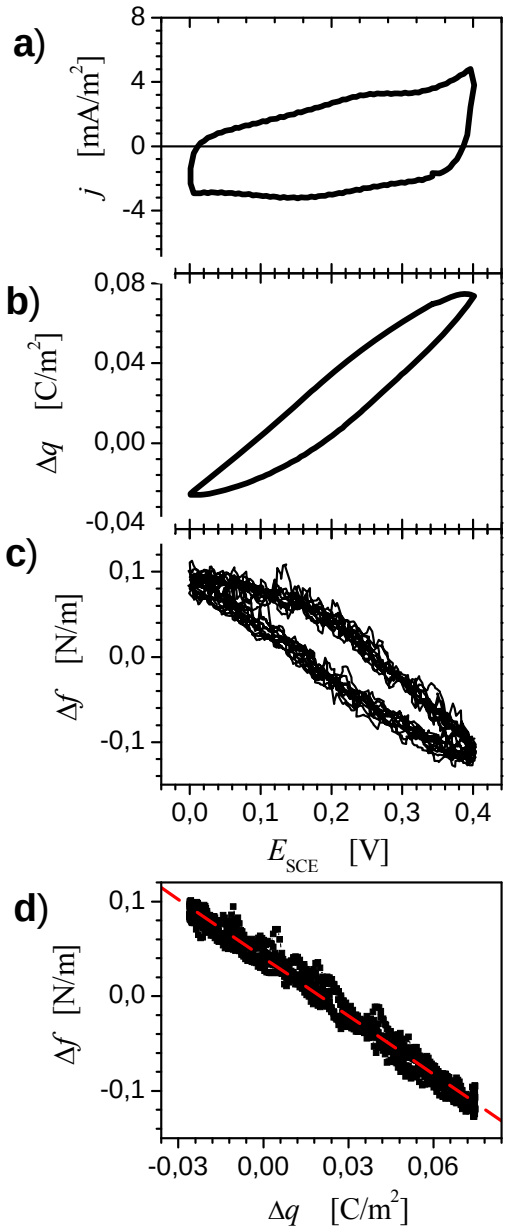

Figure 4.5. Results of the surface stress measurements of (111)-textured gold film in 7 mM NaF(aq.) (scan rate 10 mV/s). a) Cyclic voltammogram. b) Change in charge density; c) Surface stress change, Δf, versus electrode potential. d) Δf versus Δq. Line: straight dashed line of best fit, of slope -1.95 V. Parts c) and d) show 12 successive cycles superimposed.

4.3.3 Measurement of the surface stress of (111)-textured gold electrode in aqueous solution of $HClO_4$

To confirm the experimental finding of the surface stress-charge coefficient value in the base NaF aqueous electrolyte, the surface stress behaviour of the metal

was examined in acidic media. Similarly with the pervious case, the type of the working electrodes 50 nm thin (111)-textured gold film was used in the experiment.

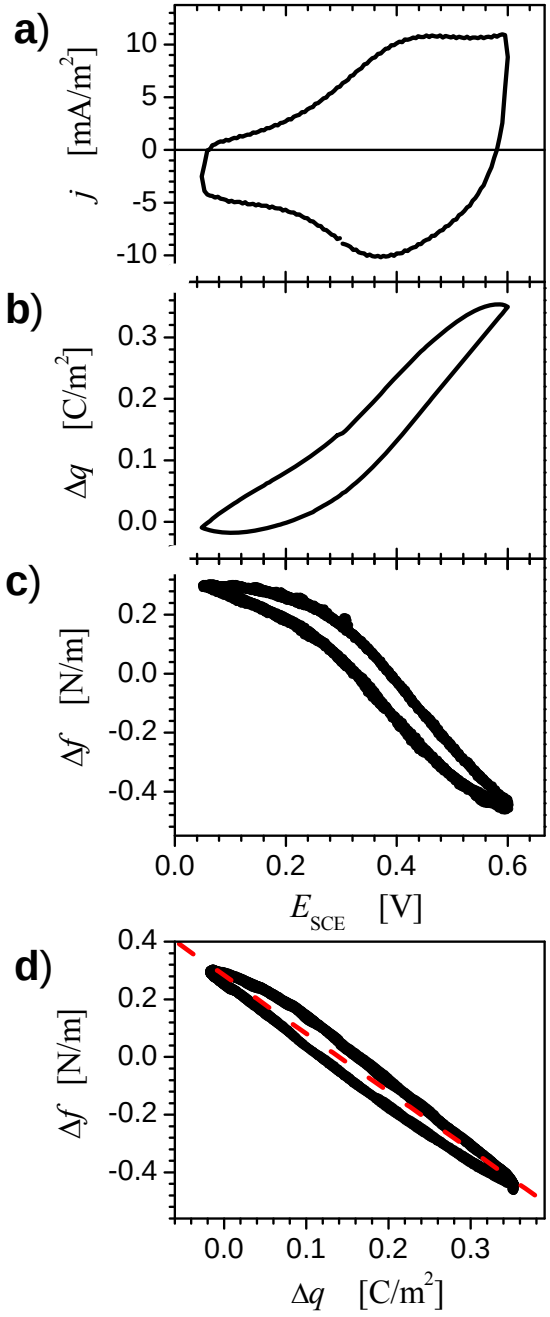

Figure 4.6 Results of the surface stress measurements of (111)-textured gold film in 10 mM $HClO_4$ (scan rate 10 mV/s). a) Cyclic voltammogram. b) Change, Δq, in charge density versus E. c) Surface stress change, Δf, versus E. d) Δf versus Δq. Line: straight dashed line of best fit. The slope is −2.01 V. Parts c) and d) show 12 successive cycles superimposed.

In analogy to Figure 4.5, Figure 4.6 shows the results of the in-situ experiment in 10 mM $HClO_4$(aq.) at 10 mV/s potential scan rate and in the potential range 0.05 to 0.6 V. Both $\Delta f(E)$ and $\Delta f(\Delta q)$ exhibit a hysteresis. Yet, $\Delta f(\Delta q)$ exhibits a reasonably linear behaviour. By applying the linear regression in the Figure 4.6, the surface

stress-charge coefficient get value of ς = (−2.01±0.02) V. The values of the ς obtained in different anions system, F^- and ClO_4^-, are in the perfect agreement.

4.3.4 Reproducibility in wafer bending experiment

The results are based on the experimental data obtained for several independent runs using several separate gold samples, each using the same procedure as the examples above. Figure 4.7 illustrates summary of the surface stress-charge coefficient value. The results are closely compatible, with a standard deviation of about 1%. When including the uncertainties in wafer thickness and optical path length (see above), we estimate the net uncertainty in ς at around 7 %. Thus, our experimental results for ς are (−1.95±0.13) V (NaF) and (−2.00±0.14) V ($HClO_4$).

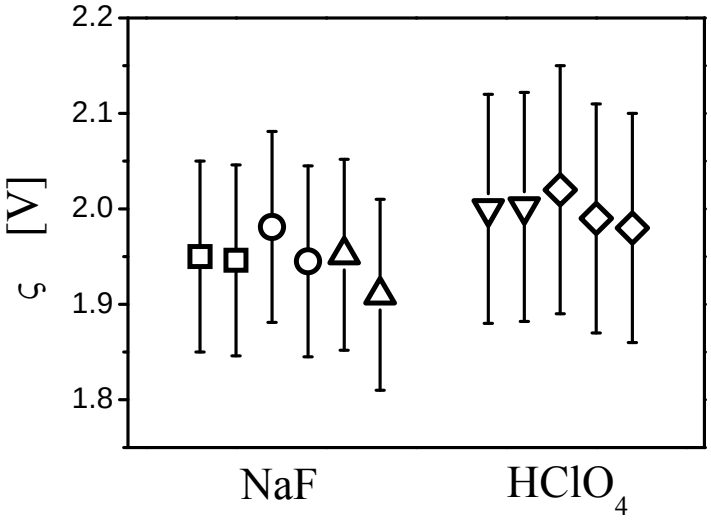

Figure 4.7 Compilation of results for the surface stress-charge coefficient, ς, in 7 mM NaF and 10 mM $HClO_4$. Each data point represents an average over 12 successive scans. Different symbols denote results obtained with different samples. Error bars represent a combination of systematic and statistical error, see text for details.

The experimental observations show that the quality of the film is crucial for the measurement. For instance, in few cases, a deviation from linearity of $f(q)$ was observed when the film started to detach from the substrate, in agreement with the observations in Ref. [10]. Furthermore, a common artifact after extended cycling (typically, for 24 hours) was a significantly decreased in the amplitudes of both f and q for a given potential interval. We find it noteworthy that, in a typical example, the two amplitudes dropped by about 30% each, whereas their ratio, ς, was reduced by only 10 %. This exemplifies that – as compared to $\Delta f/\Delta E$ – the parameter $\Delta f/\Delta q$ is significantly more robust against artifacts due to degradation of the film, provided that the charge amplitude is measured in situ, along with the surface stress variation.

4.4 Open circuit potential-strain response of Pt wire in aqueous solution of H_2SO_4

Preliminary data obtained using the balance method where a metal wire was elastically strained by manually applied a load are described in this paragraph.

Before the measurements, the electrolyte was bubbled with ultrapure argon. The gas flow was switched off during the measurement. A Pt wire of 0.1 mm diameter was repeatedly strained in 0.1 M H_2SO_4 using a load of 200 g. The open circuit potential variation during load-unload was measured versus the unstrained reference electrode (Pt wire) with a stress cycle of ca. 10 seconds, Figure 4.8. The peak-to-peak amplitude of the open circuit potential, E_{oc}, shows a good reproducibility, ΔE_{oc}=0.41±0.07 mV. The potential drift of a low frequency in the measured signal might be due to the oxygen gas present in the electrolyte. The amplitude of the applied elastic strain, e, was in order of $e = 4.5 \times 10^{-4}$. The slope of $\Delta E/\Delta e$ was calculated to be in order of –0.90 V. This experiment shows that electrode potential decreasing under the tensile stress. The measured value of $\Delta E/\Delta e$ has the same order of the magnitude and the sign as it was shown for the surface stress-charge coefficient of the nanoporous platinum in 0.1 M NaF(aq.) obtained by Viswanath et al [72].

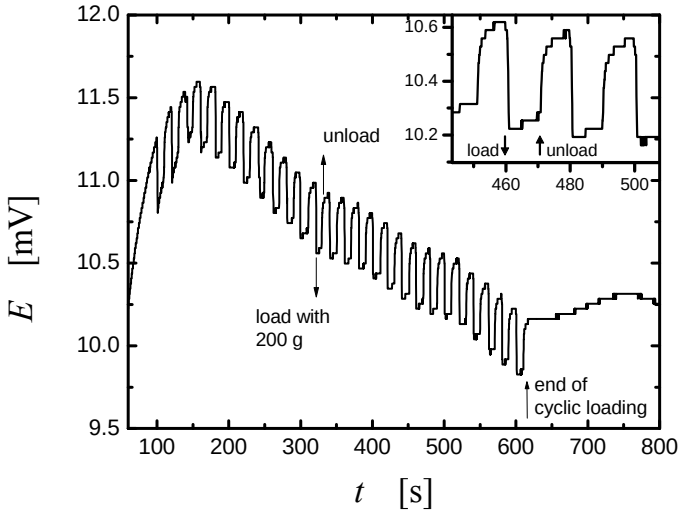

Figure 4.8 The time dependence of the platinum wire potential, E, during manual load and unload (repeated 26 times). The potential measurement occurred versus a second not stretched platinum wire. The inset shows details of the potential variation $E(t)$.

4.5 Open circuit potential-strain response of the Au film in aqueous solution of $HClO_4$

In this chapter the results of the open circuit potential response to the cyclic elastic strain, obtained with the new tension apparatus, are described. The samples, 20 nm thin (111)-textured Au film deposited on 125 μm thick Kapton foil, were used in the experiment.

4.5.1 Cyclic voltammogram of the Au electrode

A cyclic voltammogram, CV, measurements were made in order to confirm the cleanness of the sample. The typical CV for the gold surface in 10 mM $HClO_4$(aq.) is shown in Figure 4.9. The potential scan between -0.4 to 1.2 V was made at 20 mV/s. This curve is characteristic for a clean gold surface, exhibiting an essentially capacitive region of low current and an oxygen species adsorption/desorption feature at its positive end.

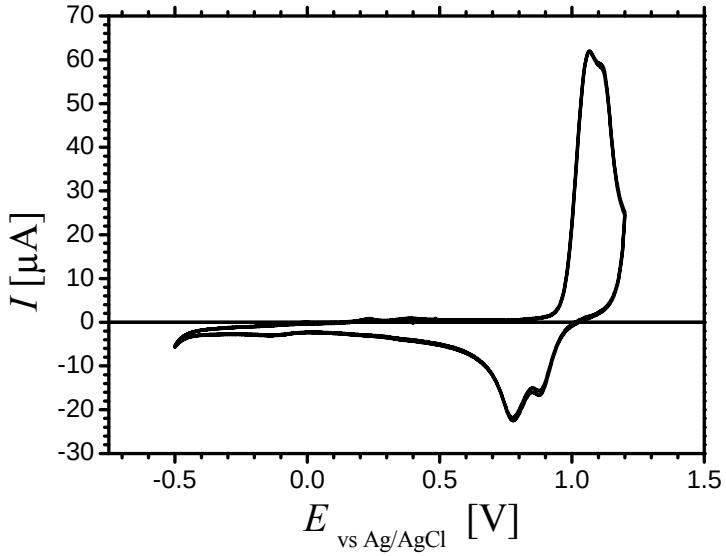

Figure 4.9. Cyclic voltammogram of 20 nm Au on Kapton foil in aqueous solution of 0.01 M $HClO_4$**.**

4.5.2 The electrode potential of a (111)-textured Au film as the function of the cyclic elastic strain

The variation of open circuit potential, E_{oc}, during the cyclic straining of the Au film was measured using chronopotentiometry method at a condition of zero current. In this method, the current between the working electrode (sample) and the counter electrode (Au wire) was set to zero. The potentiostat responds to the elastic deformation of the electrode by adjusting the potential value to satisfy zero current condition. At this current condition, the chronopotentiometry method is exact measure of open circuit potential. A sawtooth waveform of 0.5 Hz frequency and 4×10^{-4} amplitude of elastic strain, e, was applied to the sample during this measurement.

Figure 4.10a shows the E_{oc} variation recorded while the sample was cyclically strained. The electrode potential was measured versus the unstrained gold wire which has potential between 200-300 mV versus Ag/AgCl. The peak-to-peak amplitude was E_{oc}= (–0.626 ± 0.015) mV. The plot of E_{oc} versus e, Figure 4.10b, shows a linear dependency of the potential from the elastic strain with a slope of the -1.0 V for $\delta E/\delta e$. Note that the *pzc* of similar Au films in 10 mM $HClO_4$ is 245±10mV versus Ag/AgCl [Ch. 4, Figure 4.3]

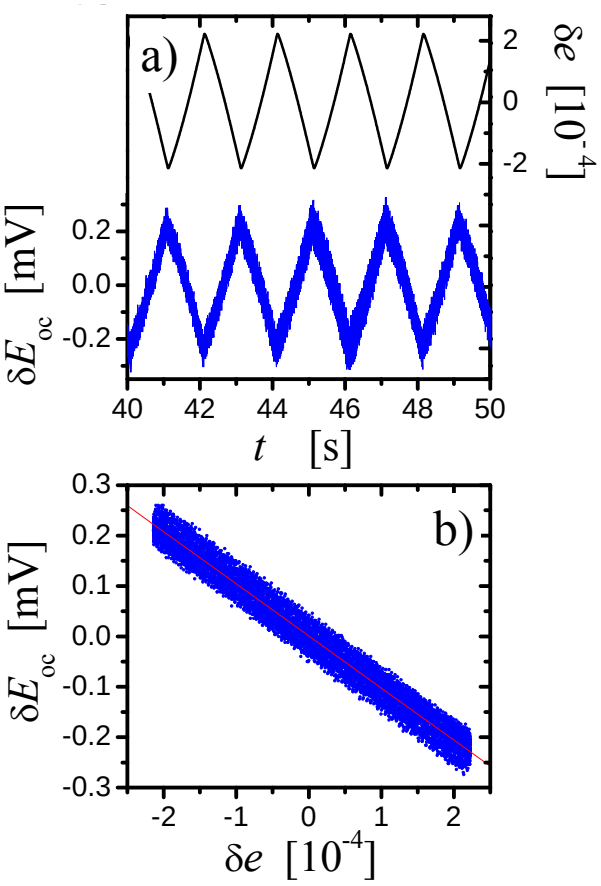

Figure 4.10. Applied cyclic strain (black line) and response in potential of the gold electrode (blue line) versus time. Gold working electrode the open circuit potential as the function of strain in 10 mM $HClO_4$(aq.) measured at 0.5 Hz of cyclic strain, versus a gold wire. 10 strain cycles are superimposed

4.5.3 Open circuit potential response at different frequencies of elastic strain of a (111)-textured Au film measured in aqueous solution of $HClO_4$

In the previous paragraph the variation of E_{oc} for the single frequency, ω, of the elastic strain was shown. The results of the variation E_{oc} measured at different frequencies and amplitudes of the elastic strain are described in this paragraph. The elastic strain frequencies was applied to the samples in the range of 0.2 – 100 Hz with the nominal amplitudes of the elastic strain in the range of $4.6x10^{-5}$ to $5x10^{-4}$. Measured δE_{oc} amplitudes and the correspondent elastic strain applied to the sample (working electrode) are shown in the Figure 4.11.

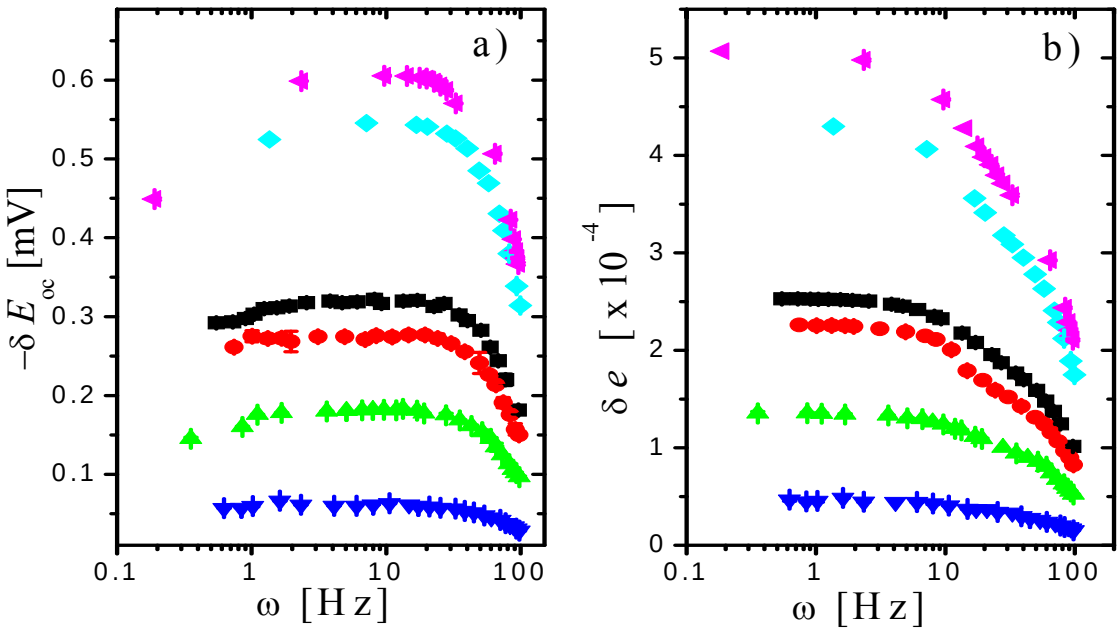

Figure 4.11. The open circuit potential response, δE_{oc}, to the elastic strain, δe, applied to the 20 nm thin Au film. Measured versus Ag/AgCl in 10 mM $HClO_4$. The nominal amplitudes of strain: ▼- 4.6×10^{-5}; ▲- 1.81×10^{-4}; ●- 2.25×10^{-4}; ■ - 2.52×10^{-4}; ◆ - 4.4×10^{-4}; ▼ -5.0×10^{-4}.

For every given frequency of the elastic strain applied to the electrode δE_{oc} was measured for at least 20 cycles. The different curves refer to different nominal strain amplitudes; the actual strain decreases at higher ω due to restrictions in the piezo-drive system.

Further, it was observed that registered by the Lock-in amplifier $\delta E_{oc}(e)$ signal had the phase shift of 180(±2)° independent from the strain frequency. This indicates that the elastic strain produces the in-phase linear response of the open circuit potential and that it has negative sign.

4.5.4 Open circuit potential-strain coefficient as a function of strain frequency of a (111)-textured Au electrode in aqueous solution of $HClO_4$

Figure 4.12 displays the open circuit potential-elastic strain coefficient, $\delta E_{oc}/\delta e$, computed from the experimental data for δE_{oc} shown in the Figure 4.11a. It is seen that all data sets collapsed into a single graph, indicating that the potential-strain response is independent of the elastic strain amplitude. This agrees with the linear behaviour of $E_{oc}(e)$ in Figure 4.10b. Furthermore, it is seen that the magnitude of the (negative-valued) $\delta E_{oc}/\delta e$ increases with increasing frequency, with an indication of a plateau at around 2 Hz. However, an apparent saturation of $\delta E_{oc}/\delta e$ at around –1.83 V value was observed beyond 40 Hz.

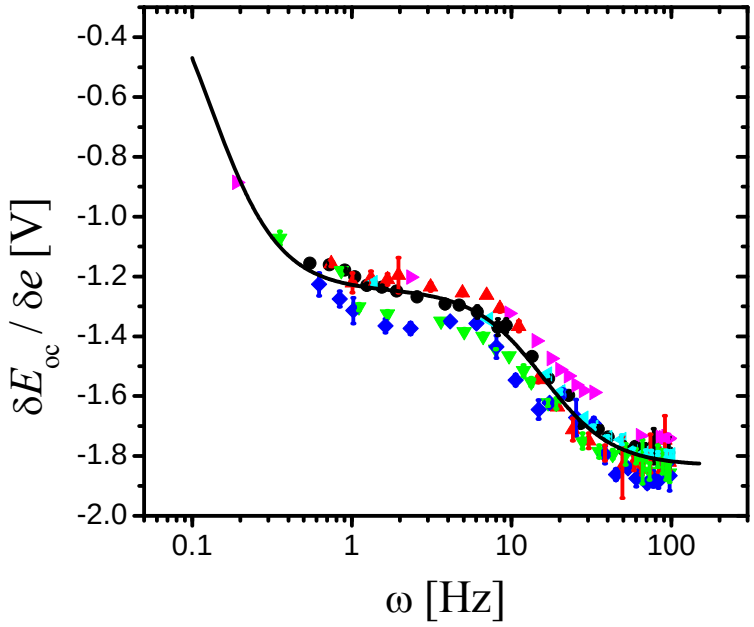

Figure 4.12. Open circuit potential-elastic strain coefficient $\delta E_{oc}/\delta e$ of 20 nm thin (111)-textured Au electrode in aqueous solution of 10 mM $HClO_4$ measured for frequencies range of the cyclic strain from 0.2 Hz to 100 Hz. Nominal magnitude of δe at frequency below 1 Hz was: ▼- 4.6×10^{-5}; ▲- 1.81×10^{-4}; ●- 2.25×10^{-4}; ■ - 2.52×10^{-4}; ◆ - 4.4×10^{-4}; ▼ -5.0×10^{-4}. Solid black line simulates $\delta E/\delta e$ curve, which was calculated using the equivalent circuit shown in Figure 4.13.

The frequency dependent character of $\delta E_{oc}/\delta e$ below 40 Hz is due to slow rate of the ions adsorption to the surface. The ions adsorption within the capacitive potential range is discharging the double layer. This discharging reduces the value of the electrode potential response to the elastic strain. The theoretical model of the experiment supports this statement. This model is discussed in the next paragraph.

4.5.5 Interpretation of the results for the $\delta E_{oc}/\delta e$ coefficient using an equivalent electrical circuit

Using of an equivalent electrical circuit for the data interpretation is widely accepted in the electrochemical impedance spectroscopy (EIS) (see for instance chapter 10 in Ref. 60). The method developed here for studying the effect of cycling elastic strain on the electrode potential has analogy with EIS. Namely, an elastic strain alternates the distance between the atoms of the electrode. The elastic strain produces the change in the work function of the metal. The electron work function and the electrode potential are two similar parameters [47]. An equivalent circuit could interpret the perturbation in the electrode potential produced by the cyclic elastic strain of different frequency. Indeed, the electrical equivalent circuit gives a clear way for an interpretation of the results. The double layer at the metal-electrolyte interface is represented by a plate capacitor. Faradaic processes happening in parallel at the metal-electrolyte interface is represented by impedance.

Let's consider the experimental results shown in the Figure 4.12. At first, the absolute value of $\delta E_{oc}/\delta e$ is increasing with the increase of strain frequency until 40

Hz, where it saturated at a value of –1.83 V. It is possible that during the longer time of a strain period i.e. ($\omega < 1$ Hz) a partial faradaic discharging of the double layer make the strain response of δE_{oc} smaller. If the cyclic strain $\omega > 40$ Hz the faradaic processes are too slow to contribute to the measured signal and $\delta E_{oc}/\delta e$ reached it maximum value.

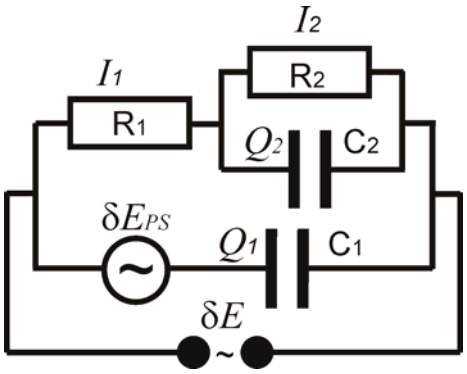

Figure 4.13 Equivalent circuit of the metal-electrolyte interface during an elastic strain- induced potential perturbation δE_{PS} and the system response δE, where C_1 is the double layer capacitance and R_2, C_2 do represent of diffusion processes.

To set up an equivalent circuit for the potential-strain experiment the simplest model was employed. This model consist of two time dependent processes, motivated in terms of the electrochemical interface properties, which have different time constants, τ_1 and τ_2. In the Figure 4.13 C_1 models the double-layer capacitance and C_2 along with the resistances R_1 and R_2 model a combination of solution resistance and Faradaic impedance. The potential-strain coupling, δE_{PS}, as the source of the potential variation at the interface is included via $\delta E_{PS}(t) = \varsigma\, e_0 \sin(\nu t)$. The circuit was analyzed for the $\delta E_{oc}(t)$ using Kirchhoff's circuit laws, finally we obtain the following linear system:

$$\begin{aligned} I_1 + \dot{Q}_1 &= 0 \\ \delta E_{PS} + \frac{Q_1}{C_1} &= \delta E_{oc} \\ \frac{Q_2}{C_2} + I_1 R_1 &= \delta E_{oc} \\ \frac{Q_2}{C_2} &= R_2 C_2 \\ I_2 + \dot{Q}_2 &= I_1 \end{aligned} \qquad 4.1$$

excluding I_1, Q_1, I_2, Q_2 from the Eq. 4.1 one get the following expression:

$$\delta E_{oc} - \left(R_2C_1 - R_2C_2 - C_1R_1\right)\delta\dot{E}_{oc} + R_1R_2C_1C_2\delta\ddot{E}_{oc} = (R_2C_1 + R_1C_1)\delta\dot{E}_{PS} + R_1R_2C_1C_2\delta\ddot{E}_{PS} \qquad 4.2$$

Taking the drive signal as $\delta E_{PS}=E_{PS}\cos(\omega t)$ a particular solution can be parameterized by a scaling factor ς, time constants $\tau_1=R_1C_1$ and $\tau_2=R_2C_2$, and the resistance ratio, $\rho = R_2/R_1$. The solution of differential equation 4.2 is correspondingly the real, δE_{ocRE}, and the imaginary, δE_{ocIM}, parts:

$$\delta E_{\mathrm{oc\,RE}} = \varsigma \frac{\tau_1 \omega^2 (\rho \tau_2 + \tau_1 (\rho^2 + \tau_2^2 \omega^2 - 1))}{((\rho-1)^2 + \tau_2^2 \omega^2)\tau_1^2 + 2(\rho-2)\tau_2 \tau_1 + \tau_2^2)\omega^2 + 1}, \quad 4.3$$

$$\delta E_{\mathrm{oc\,IM}} = \varsigma \frac{-\tau_1 \nu (\tau_2 \omega^2 (2\tau_1 - \tau_2) + \rho + 1)}{((\rho-1)^2 + \tau_2^2 \omega^2)\tau_1^2 + 2(\rho-2)\tau_2 \tau_1 + \tau_2^2)\omega^2 + 1}. \quad 4.4$$

The best fit of the real part, on the measured data displayed as the solid line in Figure 4.12, yields τ_1=0.2 s, τ_2=2.5 s, ρ = 26 and ς = –1.83 V. The model seems to provide an excellent fit to the experimental data. If $\omega < 0.5$ Hz the imaginary part is not zero, and that would mean a deviation of $E_{oc}(e)$ from linearity. However, in the experiment the open circuit potential response to the elastic strain was linear, with a phase of 180°±2° for all frequency range. Obviously, the model requires detailed description of the faradaic part, that means that it is necessary to include frequency dependent elements, like the Warburg impedance, which is relevant in the range of small frequencies. Nevertheless, the aim of the equivalent circuit is to illustrate that two types of the processes govern the $\delta E_{oc}/\delta e$ dependency from the frequency, and the model is consistent with experiments in the range of high strain frequencies.

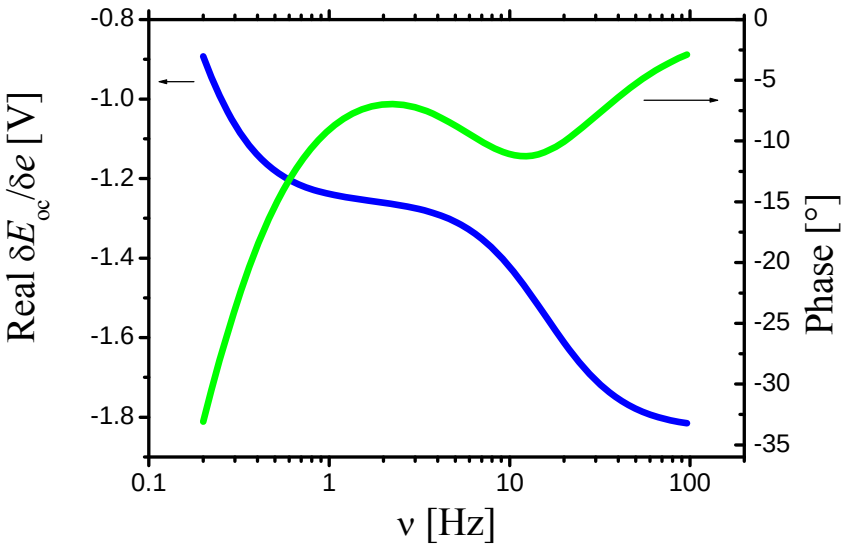

Figure 4.14. Open circuit potential-strain response calculated using an equivalent circuit shown in the Figure 4.13. The blue line is the real part and the green line is the phase.

The agreement between the real part of the model and the experimental data points towards a natural explanation of the frequency dependence of $\delta E/\delta e$: At a low frequency, the charge transfer is significant, and therefore, the measurement done not at a constant charge. With increasing frequency, the significance of this artifact is diminished, until the potential variation approximates the strain-potential response at constant charge density.

5 Discussion

5.1 The surface stress-charge coefficient of (111)-textured Au electrode in specifically nonadsorbing diluted aqueous electrolytes

5.1.1 Magnitude of surface stress-charge coefficient

A linear correlation between surface stress and charge which was found using the wafer bending method, is in agreement with previous experiments for single crystal gold surfaces in aqueous electrolytes of higher concentrations [10,73]. The present results give the value of the surface stress-charge coefficient, ς, for conditions of weak adsorption around −2.0 V. This is remarkable in view of the fact that most direct measurements of ς for Au, which have been reported so far, indicate a value that is smaller in magnitude by at least the factor of two [10,73]. Note, however, that independent observations support the larger magnitude of the present work:

i) Results in Ref. [74] – while quoting $\mathrm{d}f/\mathrm{d}E|_e$ rather than ς – are poorly compatible with the smaller magnitude of previously published ς values. In fact, $\mathrm{d}f/\mathrm{d}q$ for Au(111) can be estimated by combining data for surface stress and charge density (measured ex-situ) in Figs. 5 and 3 of that reference, respectively, using $\varsigma = c^{-1}\,\mathrm{d}f/\mathrm{d}E|_e$. In this way, we obtain about –2.3 and –2.5 V for ς in 0.1 M NaF and 0.1 M Na_2SO_4, respectively. In view of the uncertainties involved in extraction of data from the graphs and in combining data for *f* and *q* from different experiments, the result may be considered as support for our results and for the suggestion that the value of ς is closer to −2 V than to −1 V; this is confirmed for 0.1 M $HClO_4$ [75].

ii) First experiments with Pt, using more concentrated solutions, put the surface-stress charge response for that metal at ς = −0.9 V. Yet, later measurements using dilution series [27] to reduce the amount of adsorption arrived at values of larger magnitude, up to −1.9 V.

iii) Ab-initio calculation for Au(111) in vacuum suggests ς = −1.89 V [11]. This agrees closely with the present result.

iv) The results of the open circuit potential response to the elastic strain supported the newly obtained value for the surface stress-charge coefficient.

For a large value of ς at the *pzc*, the contribution to the variation of $f(q)$, which is linear in charge, is expected to dominate the $f(q)$ curve [76]. Therefore, the large ς is in agreement with our interpretation of a linear $f(q)$.

5.1.2 Presence of specific anion adsorption at the electrode

As a preliminary remark, it is emphasized that the electrolytes in question, though nominally 'weakly adsorbing', do exhibit noticeable cyclic anion adsorption/desorption during the measurements of the voltammograms. Aqueous solution of NaF was chosen because F^- ions have a low tendency for specific adsorption, due to their strongly bound solvation shell [77]. Perchloric acid is believed to have somewhat higher adsorption strength, at least at high potentials. It is still considered as weakly adsorbing close to the *pzc* [78], but a small amount of adsorption is documented in the literature [79]. For the both electrolytes, specific

adsorption is apparent in the time-dependence of the electrode behaviour: the quite different capacitances inferred from the AC experiment in Figure 4.3 (18 cycles per second) as compared to the cyclic voltammograms of Figure 4.5a and Figure 4.6a (0.02 cycles per second), suggests that some electrode processes require thermal activation, as would be expected for specific adsorption.

The observations of the hysteresis illuminate another aspect of this issue: the hysteresis of $f(q)$ in aqueous $HClO_4$ shows that the state of the electrode is here not uniquely defined by the value of q. Hysteretic specific adsorption appears to be an obvious explanation, in agreement with the statements above. By contrast, the apparent hysteresis in the voltammograms, and in particular in $q(E)$, may partly reflect the potential gradient between the reference and the working electrode, due to the uncompensated resistance of the intermediary electrolyte. Probably, this feature is therefore not, or not entirely, related to microscopic processes at the electrode, such as specific adsorption.

A relatively slow scan rate was used in the present study, namely 10 mV/s as compared to 40 mV/s [73] and even 200 mV/s [10] in previous work. Yet, inasmuch as the capacitances deduced from the voltammograms are quite similar, the difference does not seem to have a significant effect on the amount of adsorption.

5.1.3 Intrinsic surface stress-charge coefficient; role of charge transfer at metal-electrolyte interface

The excellent agreement between the present experiments and the *ab initio* computation in Ref. [11,12] suggests that the same processes may govern the surface stress-charge response at the Au-electrolyte and at the Au-vacuum interfaces. In other words, electric charge alone, without specific adsorption, can apparently cause changes of surface stress comparable to those in the experiment. The strive towards conditions of 'weak adsorption' was motivated in part by the intention to verify this picture.

The discussion of the role of adsorption based on Haiss' suggestion [10] that the surface stress variation is determined only by the effective charge density, q_M, on the metal surface, even when there is adsorption. Within our description in terms of the stress-charge coefficient, this implies that

$$\delta f = \varsigma_M \, \delta q_M , \qquad 5.1$$

where ς_M is the stress-charge coefficient of the clean metal surface. The relevant effect of specific adsorption is simply to transfer charge between the metal and the adsorbate, so that q_M may differ from the net electrode charge, q, which is experimentally accessible as the time-integral of the current in a voltammogram. F^- or ClO_4^- have been suggested [10] as good approximations to the ideal reference adsorbate with no charge transfer across the interface, so that $q_M = q$. Yet, in view of the measurable adsorption effects on the voltammogram for the corresponding electrolytes one is lead to suspect that even those weakly adsorbing ions may not entirely meet the zero charge transfer condition.

As a background for further discussion, it is useful to cast the corrections to Eq. 5.1 that take into account in the presence of adsorption into the following equations. For an ion of valence z, the possible transfer of a noninteger number λ of electrons has been described by the (electrosorption-)reaction equation [80-83]

$$\nu\ M\text{–}OH_2\ +\ S^z(aq)\ \rightarrow\ M_\nu\text{–}S^{z+\lambda}\ +\lambda e^-(met) + \nu\ H_2O(aq),$$

where S refers to the adsorbing substance. Obviously, if this reaction were to occur at constant q, it would lead to a change in the charge within the metal, q_M, that is proportional to λ and to the superficial density, Γ, of specifically adsorbed ions. It has been suggested that the dependence of the charge transfer coefficient λ on the potential is small [80] and might be neglected. Then [81]

$$q_M = q - \lambda F \Gamma, \tag{5.2}$$

where F denotes the Faraday constant. The coefficient λ is closely related to the concept of electrosorption valency. The details of this relation, which involve considerations of adsorbate position and of dipole terms of adsorbate and water, can be found in Refs. [80-83].

A nontrivial part of Haiss' hypothesis is its focus on charge-induced changes in bond forces within the metal only. In a more general scenario, it would have to be admitted that the total surface stress change contains an extra contribution, δf_Γ, due to metal-adsorbate and adsorbate-adsorbate bond forces. For instance, one might formally write $\delta f_\Gamma = (\varphi_{MA} + \varphi_{AA}\Gamma)\,\delta\Gamma$, with φ_{MA} and φ_{AA} constants representing the respective forces. Haiss' hypothesis here requires that $\delta f_\Gamma/\delta q << \varsigma_M$. The net experimental stress charge response ς could be then related to the intrinsic stress charge response ς_M and to a combination of the partial charge transfer coefficient λ and of the amount of the specific adsorption via

$$\varsigma = \frac{\delta f}{\delta q} = \varsigma_M \left(1 - \lambda F \frac{\delta\Gamma}{\delta q}\right). \tag{5.3}$$

This expression illustrates two implications of the hypothesis:

i), the surface-stress charge response might be used to estimate the charge transfer factor λ, a quantity that is notoriously difficult to access in experiments [83].

ii), experiments aiming at measuring ς_M should pursue either or both of the two strategies minimizing the net charge transfer: Use of an anion with small λ, or use of an electrolyte with low tendency for specific adsorption (small $\delta\Gamma/\delta q$).

A dependency of Γ on the anion concentration, X, in the bulk of the electrolyte must be admitted, in other words $\Gamma = \Gamma(q,X)$. Therefore, a simple scaling between ς and λ or γ cannot be inferred from Eq. 5.3. As was pointed out in Ref. [27], when both the inner Helmholtz layer and the bulk electrolyte can be approximated as dilute solutions of the adsorbing species, then Γ at a given value of E depends linearly on X. The double-layer capacitance varies more slowly, as $X^{1/2}$ according to the Gouy-Chapman theory. Thus, $\delta\Gamma/\delta q$ in Eq. 5.3 tends to zero and ς approaches ς_M in the limit of high dilution. The quite noticeable difference between the ς obtained by different authors using different X [10,24] may then suggest that a significant amount of chemisorption remains present at the higher concentrations. This is indeed confirmed by the dilution series in Ref. [27], which shows ς for Pt in NaF electrolyte to become independent of concentration only for $X < 0.1$ mol/l.

So far, experimental observations near the nominally capacitive regime of the voltammogram, allowing for weak anion adsorption, also agree with the trend predicted by Eq. 5.3: experiments with different anions find ς to be enhanced for ions with a lesser expected λ [10, 24], the dilution series finds ς to be initially enhanced and then to saturate – presumably at the value ς_M – as the dilution is increased, and the

ab initio work, which computes ς_M since adsorption is excluded, finds a large stress-charge response.

The present results for conditions of weak adsorption (small λ and small $\delta\Gamma/\delta q$), confirm the above arguments by the agreement with the *ab initio* result. Furthermore, in spite of the different adsorption behaviour of the two anions under study, practically identical ς are found. This is again consistent with Eq. 5.3, if admit that these experiments probe the limit where the correction term that represents the charge transfer has become negligible. In other words, the surface concentration of adsorbed anionic species for both electrolytes may here be so low that the excess charge in the metal indeed controls the surface stress changes.

5.1.4 Surface stress-potential response

The agreement in ς for the two electrolytes does not extend to the surface stress-potential response, $\Delta f/\Delta E$. For scans in similar potential intervals, the net change, Δf of the surface stress was 0.22 N/m in NaF, considerably less than the 0.8 N/m in $HClO_4$. Accordingly, the values of $\Delta f/\Delta E$ are 0.4 and 1.5 C/m^2, respectively, which is a difference by a factor of almost four. The finding is readily reconciled with essentially identical values of ς if the effective capacitances, $\Delta q/\Delta E$, exhibited the same difference as the $\Delta f/\Delta E$. The capacitances are governed by a combination of adsorption and of processes in the diffuse layer of the electrolyte. The ς values here appear insensitive to these processes, which are apparently noticeably different between the solutions of NaF and $HClO_4$. This is again consistent with a stress-charge response that is governed by interactions within the metal.

5.1.5 Roughness contribution to the measured surface stress

For the evaluation of the surface stress variation the generalized Stoney's formula was used (Eq. 3.5). However, the Stoney's formula is valid for the case of ideally planar surface, which is a rare case in the real experiment where a metal surface has some kind of roughness anyway. Reference[33], considered the contribution of the surface roughness into the measured surface stress within framework of the continuum mechanics.

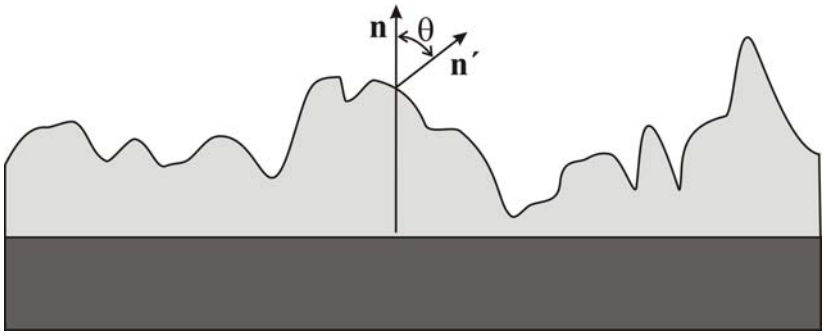

Figure 5.1. Geometry of rough surface, inclination angle θ between normal to the neutral plane **n** and normal to the surface **n´**.

Their found that the in-plane component of the mean surface stress was weakly affected by the roughness. Somewhat counterintuitively, in view of the planar stress state that is generally associated with thin films, the leading correction term arises from out-of-plane stress components which couple into the effective tangential stress due to transverse contraction. Depending on the surface inclination angle, θ, and

on the Poisson ratio, ν, of the layer, the sensitivity of the cantilever may be either increased or decreased, even to the extent where the sign of the bending is inverted.

In their model the θ and ν, of the substrate were taken as the estimate of the topological impact into the bulk stress, *T*:

$$T = \frac{\langle f \rangle}{h_f}\left(1 - \frac{\nu}{1-\nu}\langle \theta^2 \rangle\right) \qquad 5.4$$

This result illustrates that roughness affects *T* in two ways: First, the true mean value of *f* may change when inclined surface segments with modified crystallography emerge. Second, the apparent action of *f* can be reduced by a geometric effect that scales with the root-mean-square θ. Since the latter effect can be analyzed the contribution of the former can be separated, so that experiments using surfaces of varying roughness may provide insight into the variation of *f* with the surface orientation.

For small roughness, $\rho = 1 - \frac{1}{2}\langle\theta^2\rangle^{1/2}$. The Standard data analysis software in atomic force microscopy (AFM) evaluates ρ, connecting the mean-square inclination angle to experimentally accessible parameters. As an example, Figure 4.1 shows an AFM image of a 50 nm thick gold film that was used in the wafer bending study of the surface stress variation. Its analysis yields ρ = 1.061. Thus, the root-mean-square inclination angle is $\langle\theta^2\rangle^{1/2} = 2\,°$ and $-\frac{\nu}{1-\nu}\langle\theta^2\rangle = -0.095$ (based on ν=0.44 for gold), Stoney's equation in its conventional form underestimate the true mean value of the surface stress by 10%. Since the estimated relative accuracy in the surface stress response to charging is given as ±7%, the correction for roughness would introduce a meaningful change in the result which to be considered. Thus, the roughness correction applied for the surface stress-charge coefficient data obtained for the (111) textured Au yields values of (2.15±0.1) V for the NaF and (2.2±0.1) V for the $HClO_4$.

5.1.6 Summary of the charge effect on the surface stress

For Au (111) under conditions of weak adsorption there is a linear correlation between surface stress and charge in a significant potential interval around the *pzc*. Identical values for the surface stress-charge coefficients are found for two dilute aqueous electrolytes, ς = (−1.95±0.13) V in 7 mM NaF and (−2.0±0.14) V in 10 mM $HClO_4$. These values are numerically larger than some previously published ones. They do, however, exhibit good agreement with results of recent ab-initio computations for ς of Au(111) in vacuum, and with reported trends of an enhanced stress-charge response if the amount of adsorption is reduced. The hypothesis that the surface stress change is controlled by the contribution of surface excess charge to the bond forces between metal atoms in the surface and not due to forces arising from bonds with adsorbates was proven for the present experimental situation, gold in weakly adsorbing electrolytes near the *pzc*.

5.2 Electrode potential-strain response

The open circuit potential variation of a 20 nm thin gold film deposited on 125 μm Kapton was measured as the function of elastic strain in an aqueous electrolyte. Particularly, the measurements were carried out in 10 mM $HClO_4$. It was found that the elastic strain-induced potential variation is reduced by the charge transfer at the electrode combined with ionic transport through the electrolyte at the strain frequencies below 40 Hz. Under the open circuit condition the Faraday process responsible for the discharging of the double-layer reducing the potential-elastic strain response. The equivalent circuit shown in Figure 4.13 models the kinetics of these processes. With increasing frequency of the cyclic elastic strain, the significance of the faradaic discharging is decreasing, until the potential variation approximates the strain-potential response at constant charge density, the $\delta E_{oc}/\delta e$ yields value of –1.83 V. The metal-electrolyte interface free from the charge transferee processes is the interest here.

Since no direct measurement of $\delta E_{oc}/\delta e|_q$ was reported so far a comparison with results of this work could be made, in the light of other reports on df/dq or $dE/d\sigma$, where σ is tangential stress. Recent attempts to measure the potential variation during the elastic straining include the work on Ag wire in aqueous solution $AgNO_3$ by Horvath and Schiller, who report $dE/d\sigma = +2.6\times10^{-11}$ V/Pa for Ag in $AgNO_3$ [45] and the Kelvin probe experiments by Unal and Wickramasinghe for Si in dry nitrogen [84], suggesting $dE/d\sigma = -3.6\times10^{-8}$ V/Pa. By means of this comparison σ is the orientation-average scalar magnitude of the tangential stress in the bulk and account for $\sigma = B\,e/2$ with B the biaxial modulus, B = 140 GPa for Au(111). This yields $dE/d\sigma = \varsigma / B \approx -1.3\times10^{-11}$ V/Pa for the present results. Thus, the results for the sign and the magnitude of $dE/d\sigma$ differ considerably. This difference is most remarkable in relation to Ref. [45], since the electronic properties of Ag and Au are similar, so that the inversion in sign of ς is unexpected. One might tend to attribute the difference to exchange currents, since the metal in that study was present as an ion in solution. Yet, as could be argued, the contribution of exchange currents on the potential-strain response is negligible.

5.2.1 Electrode potential-strain response in an aqueous electrolyte contained metal ions

If solution contains metal ions, the equilibrium potential reached due to the exchange current at the metal-electrolyte interface. A working electrode containing N mole of metal with molar volume Ω, which can be strained tangentially to the surface is considered. Considering a planar slab geometry with a (wetted) surface area A and capacitance c, a net charge is $Q = A\,q$. The electrode geometry of the experiment enforces a constant wetted area in Lagrangian coordinates, and the same will generally apply when the electrode is completely immersed or when the electrolyte-electrode-air triple line of a partly immersed electrode adheres to the surface throughout the strain cycle. In Lagrangian coordinates, Ω and A are independent of strain [25,51]. Assuming linear elasticity in the bulk, a strain-independent surface stress value, f_0, and a linear relation between charge and potential,

$$q = c(e)\,(E - E_{zc}(e)), \qquad 5.5$$

with c the capacitance and E_{zc} the potential of zero charge, the (Helmholtz-) free energy densities of bulk (Ψ) and surface (ψ) are then

$$\Psi(e) = \Psi_0 + \tfrac{1}{2}\, B\, e^2 \qquad 5.6$$

$$\psi(e,q) = \psi_0 + f_0\, e + E_{zc}(e)\, q + \tfrac{1}{2}\, q^2 / c(e), \qquad 5.7$$

respectively. The expression for ψ is obtained by integrating work terms sequentially, first straining at $q = 0$ and then charging at constant e. The net free energy, Φ, is given by

$$\Phi = N\, \Omega\, \Psi(e) \; + A\, \psi(e,q)\; . \qquad 5.8$$

In relation to experiments with the metal ion in solution – as in Ref. 43 – for the working electrode, WE, it is allowed to exchange metal atoms, M^0, with a counter electrode, CE, of the same metal via the transport, through the electrolyte, of ions M^z of valency z. Yet, the two reactions, $M^0 \leftrightarrow M^z + ze^-$ each, at WE and CE couple N to q at open circuit via

$$A\, \delta q = z\, F\, \delta N \qquad 5.9$$

with F the Faraday constant. At a planar surface, varying N leaves the value of A invariant. The equation of state for the chemical potential, μ, of the metal in the WE is then

$$\mu = \mathrm{d}\Phi\, /\mathrm{d}N|_e = \Omega\, \Psi_0 + \tfrac{1}{2}\, \Omega\, B\, e^2 + F\, z\, E. \qquad 5.10$$

This can be ascertained by inserting Eqs. (5.6 and 5.7) into (5.8) while considering the constraint (5.9).

An idealized CE which is stress-free and of very large capacity, so that it serves at the same time as the reference for the electric and chemical potentials are considered here. In particular, the exchange of metal ions fixes the value of μ at equilibrium at the value of the counter electrode, in other words

$$\mu = \Omega\, \Psi_0\; . \qquad 5.11$$

By equating Eqs. (5.10) and (5.11), using (5.5) and solving for E, the equilibrium potential at open circuit can be obtained:

$$E_{oc} = -\tfrac{1}{2}\, B\, e^2\, \Omega\, /\, (zF), \qquad 5.12$$

so that

$$\partial E_{oc}\, /\, \partial e|_\mu = -\, B\, e\;\; \Omega\, /\, (zF)\; . \qquad 5.13$$

This equation links the E_{oc} of a stressed electrode which exchanges metal ions at equilibrium with a stress-free one to the stress magnitude, $\sigma = B\, e$. For net stresses – which are here the combined applied and residual stresses – not exceeding $\sigma = 1$ GPa the value of $B\, e\, \Omega\, /\, (zF) \leq 20$ mV, two orders of magnitude less than experimental values of ς.

The magnitude for $\partial E_{oc}/\partial e|_\mu$ predicted here was experimentally proved recently [85]. The experiment was repeated with Ag film using the identical electrolyte as in [45] (aqueous solution of 10 mM $AgNO_3$ and 0.1 M KNO_3). Open-circuit conditions were maintained at all times in order to prevent Ag film dissolution. The resulting values of $\partial E_{oc}/\partial e|_\mu$ are positive (as in [45]) for the frequencies below ~10 Hz and negative above this frequency. The $\partial E_{oc}/\partial e|_\mu$ magnitudes never exceed 25 mV, consistent with the small value of $\partial E_{oc}/\partial e|_\mu$ for the deduced from Eq. 5.13.

5.2.2 Electrode potential-strain response in a blank electrolyte

In the present experimental work the metal ions are not exchanged between the metal and the electrolyte. Here N is a constant, μ is ill-defined, and the potential variation is obtained by solving Eq. 5.5 for E and taking the derivative with respect to e at constant q:

$$\partial E / \partial e|_q = \varsigma_{zc} - q\, c^{-2}\, \mathrm{d}c/\mathrm{d}e. \qquad 5.14$$

When measured in laboratory coordinates, the capacitance for double-layer charging can be approximated as independent of e [86]. In Lagrange coordinates $c=c_0\exp(e)$, so $\mathrm{d}c/\mathrm{d}e = c$ and, with Eq. 5.5,

$$\partial E / \partial e\,|_q = \varsigma_{zc} - (E - E_{zc}). \qquad 5.15$$

As the open circuit potential in the experiment is within 50 mV of the *pzc*, the correction is negligible compared to the net value of ς=–1.83 V. Therefore, dependency of $E_{oc}(e)$ in our case is representing $E_{zc}(e)$.

5.2.3 Summary of potential-strain response results

Based on the above considerations the conclusion is the following: experiments with and without the metal ion in solution, in other words with a non-polarisable and a polarisable electrode, respectively, yield quite different results for the potential-strain response under open circuit conditions. While the response for the latter case is dominated by the linear strain-dependence of the *pzc*, that for the former case derives from a quadraatic strain-dependence of the strain energy density of the metal. It is thus not surprising that quite different results are obtained by the present experiment and Ref. [45]. Yet, the theory is not with agreement with the numerically large response reported in Ref. [45]. In relation to their positive-valued ς recent reports [87, 88] demonstrated that a metastable atomic monolayer of oxygen on Au and Pt surfaces changes ς to the extent that even the sign is inverted. This suggests that careful characterization of the surface state is indispensable for obtaining meaningful ς values. Moreover, the recent experimental observation [85] shows that the thermodynamic consideration made in the paragraph 5.2.1 is right. The experimental conditions from the Ref. [45] was repeated and the new method was applied. The magnitude of $\delta E/\delta e|_\mu$ was obtained in the order of 20 mV, as it is follows from the Eq. 5.13.

The voltammograms of the present study indicate a clean surface near the *ocp*. Significantly, the result for the open circuit potential variation with the elastic strain of the gold surface, $\delta E_{oc}/\delta e|_q = -1.83$ V, does agree well with *ab initio* calculation of the work-function strain response of Au(111) in vacuum, which indicates –1.89 V [11,12].

The value of $\delta E/\delta e$ in vacuum is also well compatible with the cantilever-bending results for the $\partial f/\partial q = -2.0$ V, discussed in the Ch. 5.1. The agreement between the experiment and the simulation of the two sides of the Maxwell relation, $\partial f/\partial q|_e = \partial E/\partial e|_q$,(Eq. 1.2) suggests that the respective approaches all provide quantitative probes for the same physics. In relation to potential-strain experiments, this study highlights the importance of the charge transfer processes at the metal-electrolyte interface.

6 Summary

The main achievement of the work is the experimental validation of the thermodynamic Maxwell relation. The Maxwell relation states the equality between the two important parameters of the surface energy density – the surface stress-charge coefficient, $\mathrm{d}f/\mathrm{d}q$, and the electrode potential-elastic strain response, $\mathrm{d}E/\mathrm{d}e$.

The first quantitative result on the electrode potential-elastic strain response was provided with the newly developed experimental method. This experiments show that the intrinsic value of the open circuit potential-elastic strain response, $\mathrm{d}E/\mathrm{d}e|_q$, of the gold film in $HClO_4$(aq.) was –1.83 V. Moreover, the cantilever-bending experiment shows that the surface stress-charge coefficient, $\mathrm{d}f/\mathrm{d}q|_e$, of the gold film was –1.95 V for 7 mM NaF(aq.) and –2 V for 10 mM $HClO_4$(aq.). Therefore, the equality between the surface stress-charge coefficient and electrode potential-elastic strain response, $\mathrm{d}f/\mathrm{d}q|_e = \mathrm{d}E/\mathrm{d}e|_q$, was experimentally proved the thermodynamic Maxwell relation for the first time.

The cantilever bending study of the metal-electrolyte interface shows that the surface charge and not the adsorption affects the surface stress variation of a metal. The main strive in this part of the experimental study was to have ideal conditions of – capacitive charge, with substantially minimized amount of specific anions adsorption. This was achieved by selection weakly adsorbing and highly diluted aqueous electrolytes: the aqueous solutions of NaF and $HClO_4$. The experiments show that in both electrolytes the surface stress of a (111) textured gold film varies linearly with the surface charge. However, a some difference between the positive and negative scan directions of the charge was present in the $f(q)$ curve measured in 10 mM $HClO_4$(aq.). The presence of the specific anion adsorption is one of the possible origins of the hysteresis in the $f(q)$. Strong solvation shell of perchlorate anions do not allow them specifically adsorbs to the surface. Although, a tendency for specific adsorption of perchlorate ions to a metal surface is possible [78]. This specific adsorption causes the charge transfer in the electric double layer. The charge transfer and capacitive charging processes could not be differentiated during the cyclic voltammetry experiment. Therefore, intrinsic charge in the metal, induced by the diffuse layer, might be different compare with the charge integrated from CV. Importantly, the $f(q)$ curve measured for gold surface in diluted aqueous NaF was perfectly linear and independent from the scan directions. Fluoride anions in aqueous solution have very strong solvation shells. The strong solvation shell blocks them from being specifically adsorbed on the surface, thus the charge measured by CV in diluted aqueous NaF is very close to the intrinsic charge in the metal. Therefore, the deviation of the surface stress-charge dependency from the linear behaviour seen in the case of the $f(q)$ measured for gold in 10 mM $HClO_4$(aq.), could provide information about the charge transfer and the amount of specific adsorption. This quantitative information about the amount of the charge transfer is not yet accessible by other experiments.

The observation the different role in the surface stress of the intrinsic charge and the charge transfer at the metal-electrolyte interface was proven by the alternative method. The second experimental method was developed during this work. The task

was to have precise and quantitative measurements of the electrode potential as the function of the elastic strain. The (111) textured gold film deposited on a polyimide substrate was immersed into the aqueous electrolyte and subjected to the cyclic elastic strain of different frequencies and amplitudes. The result of this experiment is that the potential of the gold electrode linearly depends from the elastic strain. The linearity of $E(e)$ was independent of the applied frequencies and amplitudes of the elastic strain. However, the magnitude of dE/de shows dependency from the frequencies of the elastic strain. The absolute magnitude of dE/de was increasing until the frequency reached 30 Hz. For the frequency higher then 30 Hz the value of dE/de saturates at –1.83 V. The electric equivalent circuit models the kinetics of these processes. The agreement between model and experimental data points towards a natural explanation of the frequency dependence of dE/de: The strain-induced potential variation is reduced by Faraday charge transfer at the electrode combined with ionic transport through the electrolyte. Under the open circuit condition that characterizes the experiment the Faraday process discharges the double-layer, thereby reducing the potential variation. At low frequency, the transport is significant and therefore the measurement is not at constant charge. With increasing frequency, the significance of this artifact is diminished, until the potential variation approximates the strain-potential response at constant charge density. Therefore, this experimental result supports the statement about the main contribution of the intrinsic charge to the surface stress of the metal.

The newly developed method of studying the electrode potential dependency from the elastic strain has an important extension. It was becomes possible to measure the amplitude of the electrode potential response during the linear cycling of the electrode potential. In particular, the magnitude of dE/de at the different values of electrode potential is not known yet. This information could provide straightforward evidence of the coupling between the elastic strain and catalytic reactivity of the metal surface [7,8,9]. In opposite to static methods used to impose the elastic strain to the metal surface by using the mismatch in the crystal lattice between a substrate and an adlayer film, Refs. [7,8,36], in the new approach the elastic strain applies directly to the surface. This is excluding the contribution from the substrate into the electronic states of the surface. Therefore, the pure effect of the crystal lattice variation into the surface reactivity could be studied. This is ongoing research project, the preliminary results shown in outlook.

Furthermore, an important point was made concerning the surface stress measurements of a rough surface in Ref. [33]. Applying the roughness correction to our results the true value of the surface stress can be by 10 % higher then the measured value and consequently the surface stress coefficient can be increased by 10 %.

7 Outlook: Potentiostatic measurement of the potential-strain response

As it was shown in Ref. [38] the elastic strain exerted on the surfaces tune the catalytic reactivity. Most of the experimental methods so far offering the static surface deformation which is produced because of the misfit between a substrate and an adlayer [39].

The experimental method presented in this work for the measurement of the $\partial E_{oc}/\partial e|_q$ at the metal-electrolyte interface is possible to extend in order to directly study the influence of the elastic strain of the electrode onto electrochemical reactivity of the metal surface. This is achievable if the potential or the current oscillations measured during the cyclic elastic strain at given electrode potential values, $\Delta E/\Delta e|_E$. The example of the $\Delta E/\Delta e|_E$ measurement presented in the Figure 7.1, where during the CV the amplitude of the $\Delta E(e)$ is determined.

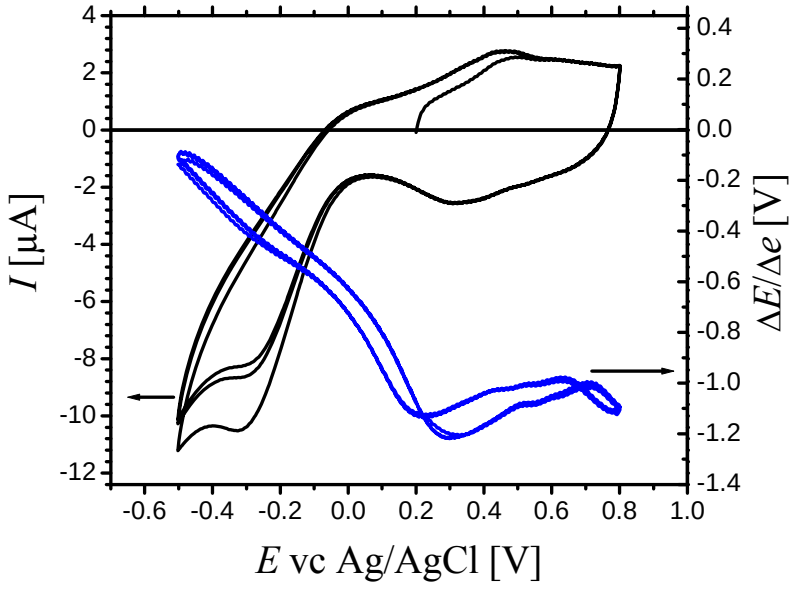

Figure 7.1 Measurement of $\partial E/\partial e|_E$ coefficient during the CV of (111) textured Au in 10 mM H_2SO_4(aq.).

One could see that in the double layer region, in the range of 0.2 V to 0.8 V, the coefficient has value of about –1.1 V, with the maximum value of –1.25 V at 0.3 V. In the range of –0.5 V to 0.2 V the absolute amplitude of $\Delta E/\Delta e$ response is gradually decreasing. The maximum value of the $\Delta E/\Delta e$ could associated with the *pzc*.

Symbols

Symbol	Meaning	Units
f	surface stress	N/m
γ	surface tension	N/m
e	strain	
E	electrode potential	V
E_{oc}	open circuit potential	V
E_{zc}	potential of zero charge	V
q	charge density	C/cm²
ς	surface stress-charge coefficient	V
$\varsigma_{м}$	intrinsic surface stress-charge coefficient	V
Ψ	Helmholtz free energy of bulk	J/cm²
ψ	Helmholtz free energy of surface	J/cm²
μ	electrochemical potential	J
F	Faraday constant/ charge on one mole of electrons	C
Γ	superficial density of specifically adsorbed ions	mol/cm²
ν	Poisson ratio	
T	bulk stress	N/m²
σ	tangential bulk stress	N/m²
ρ	roughness factor	
θ	surface inclination angle	radian
ω	frequency	Hz
pzc	potential of zero charge	
ocp	open circuit potential	
aq.	aqueous solution	

References

1 H. Helmholtz, *Pogg.Ann.* **LXXXIX**, 211 (1853)

2 J.W. Gibbs, *Collected Works* (1948) (New Haven, CT: Yale University Press)].

3 G. Lippmann, *Ann. Chim. Phys.,* **5** (1875) 494

4 G. Gouy, *J. Phys .Radium,* **9** (1910) 457; G. Gouy, *Compt. Rend*., **149** (1910), 654

5 D. L. Chapman, *Phil .Mag.*, **25** (1913) 475

6 H. Ibach, Electrochim. Acta, **45** (1999) 575–581

7 E. Kampshoff, E. Hahn, and K. Kern, Phys. Rev. Lett. **73** (1994) 704

8 M. Gsell, P. Jakob, and D. Menzel, Science **280** (1998) 717

9 M. Mavrikakis,1 B. Hammer, and J. K. Nørskov. *Phys. Rev. Lett*., **81** (1998) 2819

10 W. Haiss, R.J. Nichols, J.K. Sass, K.P. Charle, *J. Electroanal. Chem.,* **452** (1998) 199–202

11 Y. Umeno, C. Elsässer, B. Meyer, P. Gumbsch, M. Nothacker, J. Weissmüller, F. Evers, *Europhys Lett.*, **78** (2007**)** 13001-p1

12 F. Weiegend, F. Evers and J. Weissmueller, *Small*, **2** (2006) 1497

13 A.Y. Gokshktein, Surface tension of a solid body and adsorption, Nauka, Moscow (1976)

14 T. G. Thundat, E. A. Wachter, U.S. Patent 5,719,324, filed June 16,

15 A. M. Moulin, S. J. O'Shea, M. E. Welland, *Ultramicroscopy,* **82**(2000) 23–31.

16 J. Fritz, M. K. Baller, H. P. Lang, H. Rothuizen, P. Vettiger, E. Meyer, H.-J. Güntherodt, Ch. Gerber, J. K. Gimzewski, *Science*, **288** (2000) 316–318.

17 V. Tabard-Cossa, M. Godin, L. Y. Beaulieu, P. Gru¨tter, *Sens. Actuators,B*, **107** (2005) 233–241.

18 D. Kramer. R.N. Viswanath and J. Weissmüller, *Nano Lett.*, **4** (2004) 793

19 J. Weissmüller, R.N. Viswanath, D. Kramer, R, Würschum and H. Gleiter, Science, **300** (2003) 312

20 Concentris GmbH, Basel, Switzerland, offers micromechanical silicon cantilever arrays, a functionalisation unit and a cantilever sensor platform (Cantisens).

21 D. Sander and H. Ibach, Phys. Rev. B, **43** (1991) 4263-7

22 A.J. Schellsorokin and R.M Tromp, Phys.Rev. Lett., **64** (1990) 9

23 G. Stafford, U. Bertocci, J. PHYS. CHEM. C, **113** (2009) 13249

24 W. Haiss, Rep. Prog. Phys., **64** (2001) 591

25 J. Weismüller, D. Kramer, Langmuir, **21**(2005) 4592

26 W. Haiss, Rep. Prog. Phys., **64** (2001) 591

27 R.N. Viswanath, D. Kramer, J. Weissmüller, Langmuir, **21**(2005) 4604

28 T.R. Beck „Electrocapillary Curves" of Solid Metals Measured by Extonsiometer Instrument, J. Phys. Chem., **73** (1969) 466

29 M. Smetanin, R.N. Viswanath, D. Kramer, D. Beckmann, T. Koch, L.A. Kibler, D.M. Kolb, J. Weissmüller, Langmuir, **24** (2008), 8561.

30 C. Friesen, N. Dimitrov, R. C. Cammarata, K. Sieradzki, *Langmuir*, ***17***(2001**)** 807–815.

31 Th. Heaton, C. Friesen, *J. Phys. Chem. C*, **111** (2007) 14433–39.

32 K.J. Vetter, J. Schultze, *Berichte Bunsenges. Phys. Chem.* **76** (1972) 920–927

33 J. Weissmüller, H.L. Duan, *Phys. Rev.Lett.*, **101** (2008) 146102

34 W. Thompson, *Trans. Roy. Soc*., **146** (1856) 649

35 A.V. deForest, *Instruments,* **15** (1942) 848

36 L.A. Kibler, E. M. El-Aziz, R. Hoyer and D. M. Kolb, Angew. Chem., Int. Ed., **44** (2005) 2080.

37 A. Ruban, B. Hammer, P. Stoltze, H.L Skriver.and J.K Nørskov, J. Mol. Catal. A, **115** (1997) 421

38 M. Mavrikakis,1 B. Hammer, and J. K. Nørskov. Phys. Rev. Lett., **81** (1998) 2819

39 L.A. Kibler, E. M. El-Aziz, R. Hoyer and D. M. Kolb, Angew. Chem., Int. Ed., **44** (2005) 2080.

40 R. H. Jones, Stress-Corrosion Cracking: Materials Performance and Evaluation, ASM International, Materials Park, Ohio, 1992.

41 H. Gerischer, Elektrochemische Vorgänge bei der Spannungskorrosion, Werkstoffe u. Korrosion, **8(7)** (1957) 394–401

42 A. R. Despic, R. G. Raicheff, J. O'M. Bockris, Mechanism of the Acceleration of the Electrodic Dissolution of Metals during Yielding under Stress, J. Chem. Phys., **49(2)** (1968) 926–938

43 M. Seo, X. C. Jiang and N. Sato, *J. Electrochem. Soc.*, **134** (1987) 3094

44 R.E. Fryxell, N.H. Nachtrieb, J. Electrochem. Soc., **99** (1952) 495.

45 Á. Horváth, R. Schiller, Phys. Chem. Chem. Phys., **3** (2001) 2662.

46 S. Trasatti, J. Electroanal. Chem., **33** (1971) 351

47 D.L. Rath and D.M. Kolb, Surf. Sci., **109** (1981) 641

48 K. Sieradzki, R.C. Newman, Philosophical Magazine A, **51** (1986) 95

49 J.W. Gibbs The collected Works of J.W. Gibbs; Longmans, Green and Co.: New York 1928; Vol.**I**; pp 224-229

50 R. Shuttleworth, The Surface Tension of Solids, Proc. Phys. Soc., London, Sect. A, **63** (1950)444

51 J.W. Cahn, In Interfacial Segregation; W.C. Jonson, J.M. Blakely, Eds.; ASM: Metals Park, OH 1979-3

52 J. Weissmüller, J, Phys. Chem. B, **106** (2002) 189

53 G. G. Stoney, *Proc. R. Soc. A***, 82** (1909) 172–175.

54 R.Koch and R.Abermann, Thin Solid Films, **129** (1985) 63

55 H.Ibach, Phys. Status Solidi, **31** (1969) 625

56 R.A. Fredlein, A. Damjanovic and J.O.M. Bockris, Surf. Sci., **25** (1971) 261-4

57 R.A. Fredlein and J.O.M. Bockris, Surf. Sci., **46** (1974) 641

58 J. A. Floro and E. Chason, *Mater. Res. Soc. Symp. Proc.*, **406** (1996**)** 491–496.

59 J. A. Floro, E. Chason, S. R. Lee, R. D. Twesten, R. Q. Hwang, L. B. Freund, *J. Electron. Mater.*, **26** (1997) 969–979.

60 A.J. Bard and L.R. Faulkner, Electrochemical Methods, sec. ed. Wiley, **2001**

61 A.N. Frumkin, O.A. Petrii, B.B. Damaskin, in: J.O'M. Bockris, B.E. Conway, E. Yeager (Eds.), Comprehensive Treatise of Electrochemistry, vol. 1, Plenum Press, New York, 1980 (Chapter 5)

62 S. Trasatti, in: J.O'M. Bockris, B.E. Conway, E. Yeager (Eds.), Comprehensive Treatise of Electrochemistry, vol. 1, Plenum Press, New York, 1980 (Chapter 2)

63 A. Hamelin, L. Stoicoviciu, *J. Electroanal. Chem.* **234** (1987) 93.

64 G. Valette, *J. Electroanal. Chem*. **269** (1989) 191

65 S. Trasatti, *Surf. Sci.,* **335** (1995)1

66 W. A. Brantley, *J. Appl. Phys.,* **44** (1973) 534–535.

67 K. Dahmen, S. Lehwald, H. Ibach, *Surf. Sci.*, **446** (2000) 161–173.

68 D. Dickertmann, F.D. Koppitz and J.W. Schultze, *Electrochim. Acta*, **21** (1976) 967–971.
A. Hamelin, in B.E. Conway, R.E. White and J.O'M. Bockris (Eds.), *Modem Aspects of Electrochemistry*, Vol. 16, Plenum, New York, 1987.

69 B. Özkaya, S.R. Saranu, S. Mohanan, U. Herr, Phys. Stat. Sol. (a), **205** (2008) 1876.

70 Summary of properties for Kapton polyimide films, DuPont©

71 D.M. Kolb and J. Schneider, *Electrochim. Acta*, **31**(1986) 929–936.

72 R. N. Viswanath,D. Kramer, and J. Weissmüller, *Langmuir,* **21** (2005) 4604

73 H. Ibach, C.E. Bach, M. Giesen, A. Grossmann, *Surf. Sci.*, **375** (1997**)** 107–119

74 N. Vasiljevich, T. Trimble, N. Dimitrov, K. Sieradzki, *Langmuir* **20** (2004) 6639

75 V. Tabard-Cossa, M. Godin, I. J. Burgess, T. Monga, R. B. Lennox, P. Grütter, *Anal. Chem.*, **79** (2007) 8136–8143

76 D. Kramer, *Phys. Chem. Chem. Phys.*, **10** (2008) 168–177.

77 J. O'M Bockris, A. K. N. Reddy, *Modern Electrochemistry*, Vol. 2; Plenum Press, New York, 1970, p. 744.

78 A. Hamelin, T. Vitanov, E. Sevastyanov, A. Popov, *J. Electroanal. Chem.*, **145** (1983) 225–264.

79 A. Hamelin, *J. Electroanal. Chem.*, **210** (1986) 303–309.

80 K. J. Vetter, J.Schultze, *Berichte Bunsenges. Phys. Chem.*, **76** (1972**)** 920–927.

81 J.W. Schultze, D. Rolle, *J. Electroanal. Chem.*, **552** (2003) 163–169.

82 P.A. Rikvold, Th. Wandlowski, I. Abou Hamad, S.J. Mitchell, G. Brown, *Electrochim. Acta*, **52** (2007) 1932–1935

83 J.W. Schultze, K.J. Vetter, *J. Electroanal. Chem.*, **44** (1973) 63–81.

84 K. Unal, H.K. Wickramasinghe, *Appl. Phys. Lett*., **90** (2007) 113111.

85 M. Smetanin, Q. Deng, D. Kramer, S. Mohanan, U. Herr, J. Weissmüller, *Phys. Chem. Chem. Phys.* (2010) DOI:10.1039/C001731K.

86 D. Kramer, J. Weissmüller, *Surf. Sci.,* **601** (2007) 3042.

87 R.N. Viswanath, D. Kramer, J. Weissmüller, *Electrochim.Acta,* **53** (2008)2757.

88 H.J. Jin, S. Parida, D. Kramer, J. Weissmüller, *Surf. Sci.,* **602** (2008) 3588.